university of groningen

University Medical Center Groningen

University of Groningen

Single-molecule studies of the conformational dynamics of ABC proteins

de Boer, Marijn

DOI:
10.33612/diss.125779120

IMPORTANT NOTE: You are advised to consult the publisher's version (publisher's PDF) if you wish to cite from it. Please check the document version below.

Document Version
Publisher's PDF, also known as Version of record

Publication date:
2020

Link to publication in University of Groningen/UMCG research database

Citation for published version (APA):
de Boer, M. (2020). *Single-molecule studies of the conformational dynamics of ABC proteins*. [Thesis fully internal (DIV), University of Groningen]. University of Groningen. https://doi.org/10.33612/diss.125779120

Copyright
Other than for strictly personal use, it is not permitted to download or to forward/distribute the text or part of it without the consent of the author(s) and/or copyright holder(s), unless the work is under an open content license (like Creative Commons).

The publication may also be distributed here under the terms of Article 25fa of the Dutch Copyright Act, indicated by the “Taverne” license. More information can be found on the University of Groningen website: https://www.rug.nl/library/open-access/self-archiving-pure/taverne-amendment.

Take-down policy
If you believe that this document breaches copyright please contact us providing details, and we will remove access to the work immediately and investigate your claim.

Downloaded from the University of Groningen/UMCG research database (Pure): http://www.rug.nl/research/portal. For technical reasons the number of authors shown on this cover page is limited to 10 maximum.

Download date: 05-05-2023

2

Conformational and dynamic plasticity in substrate-binding proteins underlies selective transport in ABC importers

Marijn de Boer, Giorgos Gkouridis, Ruslan Vietrov, Stephanie L. Begg, Gea K. Schuurman-Wolters, Florence Husada, Nikolaos Eleftheriadis, Bert Poolman, Christopher A. McDevitt and Thorben Cordes

eLife 8, e44652 (2019)

Substrate-binding proteins (SBPs) are associated with ATP-binding cassette (ABC) importers and switch from an open to a closed conformation upon substrate binding. We investigated the effect of substrates on the conformational dynamics of six SBPs and the impact on transport. Using single-molecule FRET, we reveal an unrecognized diversity of plasticity in SBPs. We show that a unique closed SBP conformation does not exist for transported substrates. Instead, SBPs sample a range of conformations that activate transport. Certain non-transported substrates leave the structure largely unaltered or trigger a conformation that is distinct from that of transported substrates. Intriguingly, in some cases, similar SBP conformations are formed by both transported and non-transported substrates. In this case, the inability for transport arises from slow opening of the SBP or the selectivity provided by the translocator. Our results reveal the complex interplay between substrate-SBP interactions, SBP conformational dynamics and substrate transport.

2.1 Introduction

ATP-binding cassette (ABC) transporters facilitate the unidirectional trans-bilayer movement of a diverse array of molecules using the energy released from ATP hydrolysis[1]. ABC transporters share a common architecture, with the translocator unit comprising two transmembrane domains (TMDs), which form the translocation pathway for the substrate, and two cytoplasmic nucleotide-binding domains (NBDs), which bind and hydrolyse ATP (Figure 1.1). ABC importers require an additional extra-cytoplasmic accessory protein referred to as a substrate-binding protein (SBP)[2-4]. ABC importers that employ SBPs can be subdivided as Type I or II based on structural and mechanistic distinctions[5, 6]. A unifying feature of the transport mechanism of Type I and II ABC importers is the binding and delivery of substrate from a dedicated SBP to the translocator unit for import into the cytoplasm (Figure 1.7).

Prokaryotes use multiple distinct ABC importers to facilitate the acquisition of essential nutrients such as sugars, amino acids, peptides, vitamins and metal ions[1, 7]. Many ABC importers can transport more than one type of substrate molecule using high affinity interactions between the SBP and the transported substrate (herein termed cognate substrates)[2]. Despite the low sequence similarity between SBPs of different ABC importers, they share a common architecture comprising two structurally conserved subdomains connected by a flexible hinge region (Figure 2.1)[2]. Numerous biophysical[8] and structural analyses[9] indicate that substrate binding at the interface of the two subdomains facilitates switching between two conformations, i.e., from an open to a closed conformation. Bending and unbending of the hinge brings the two subdomains together (closed conformation) or apart (open conformation), respectively (Figure 1.5). Crystallographic analysis shows that the amount of opening varies between different SBPs. The subdomain-movements observed range from small rearrangements as in the SBP BtuF[10], to complete reorientation of both subdomains by angles as large as 60° in the SBP LivJ[11]. Nevertheless, the wealth of structural data permits a structural classification of SBPs, wherein the hinge region is the most defining feature of each cluster (Figure 2.1)[2, 3]. Crystal structures of the same protein, but with different substrates bound, generally report the same degree of closing of the SBP[11-15].

It is assumed that the conformational switching of the SBPs enables the ABC transporter to allosterically sense the loading state of the SBP-substrate complex ('translocation competency'), thereby contributing to the transport specificity[7, 9]. For example, crystal structures of the SBP MalE (also termed maltose-binding protein or MBP) show that the protein adopts a unique closed conformation when interacting with cognate substrates maltose, maltotriose and maltotetraose[15], while the non-transported substrate β-cyclodextrin is bound by MalE[16, 17] but cannot induce full closing[17-19]. Substrates that are bound by the

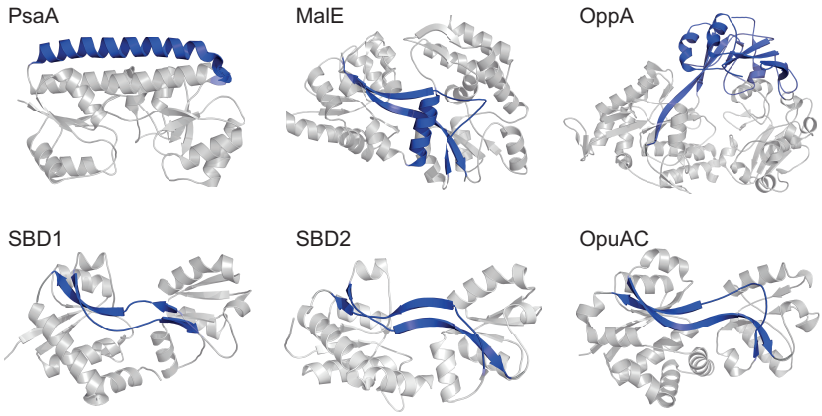

Figure 2.1. Representative SBPs from different structural clusters, categorized by their hinge region. X-ray crystal structures of PsaA (3ZK7; cluster A), MalE (1OMP; cluster B), OppA (3FTO; cluster C), OpuAC (3L6G; cluster F), SBD1 (4LA9; cluster F) and SBD2 (4KR5; cluster F) are all shown in the open substrate-free conformation. Hinge regions are shown in blue and the two rigid lobes in grey. For classification of the proteins in clusters see Berntsson et al. and Scheepers et al.[2, 3].

SBP, but cannot be transported, are termed herein non-cognate substrates. Such findings suggest that only SBPs that adopt the closed conformation can productively interact with the translocator and initiate transport. However, the TMDs of certain ABC importers were also shown to interact directly with their substrates. In $MalFGK_2E$[20] from *Escherichia coli* and $Art(QM)_2$[21] from *Thermoanaerobacter tengcongensi* substrate-binding pockets have been identified inside the TMDs, and these might be linked to the regulation of transport. Similar binding pockets within the TMDs have not been observed in the high-resolution structures of other ABC importers, although cavities through which the substrate passes in the transition of the TMD from outward- to inward-facing must be present in all the transporters[22-24]. Additional complexity exists for the coupling of SBP conformational switching and the substrate recognition process, as crystallographic[25, 26], nuclear magnetic resonance (NMR)[27] and single-molecule[28, 29] studies indicate that SBPs undergo conformational changes in the absence of substrate. Furthermore, crystal structures of the SBPs MalE and a D-xylose SBP in an open substrate-bound conformation were obtained[30, 31]. Such observations question the precise relationship between SBP-substrate interactions, SBP conformational changes and their involvement in transport function.

A range of biophysical and structural approaches have already been used to decipher the mechanistic basis of SBP-substrate interactions[8, 9, 11, 17, 19]. However, these techniques only provide information on the overall population of molecules. Recent advances in single-molecule methodologies now permit new insight into the conformational heterogeneity, dynamics and occurrences of rare events in SBPs and other proteins[28, 29, 32-35], which are difficult to obtain in bulk measurements. Here, we combined single-molecule Förster

resonance energy transfer (smFRET)[36] and transport measurements to investigate how cognate and non-cognate substrates influence the conformational states and the underlying dynamics of SBPs. Six distinct SBPs were selected (Figure 2.1)[37-41], based on two criteria. First, they cover the breadth of SBP structural classes: PsaA (cluster A), MalE (cluster B), OppA (cluster C), SBD1 and SBD2 of GlnPQ, and OpuAC (all cluster F). The selected SBPs provide coverage of hinge region diversity[2, 3], thereby addressing a hypothesized key determinant in SBP conformational dynamics. Moreover, subtle structural or sequence differences among SBPs that belong to the same cluster are addressed by examining SBD1, SBD2 and OpuAC that all belong to cluster F. Second, the selected SBPs belong to Type I and II importers with extensively characterized substrate (cognate and non-cognate) interactions, such as metal ions (PsaA)[40], sugars (MalE)[42], peptides (OppA)[43], amino acids (SBD1 and SBD2)[37] and compatible solutes (OpuAC)[38].

2.2 Results

2.2.1 Multiple SBP conformations are translocation competent

Crystal structures of SBPs suggest that substrate binding is coupled to switching between two protein conformations, an open and a closed conformation. Mechanistically, this process has been linked to the allosteric regulation of substrate transport[7-9, 44-48]. Here, we assessed this model by investigating the interaction of six SBPs, PsaA, MalE, OppA, SBD1, SBD2 and OpuAC, with a range of cognate substrates. We employed single-molecule FRET to analyse the SBP conformations, wherein each of the two SBP subdomains was labelled with either a donor or an acceptor fluorophore (Figure 2.2A)[29, 49]. Surface-exposed and non-conserved residues, showing largest distance changes according to the crystal structures of the open and closed states, were chosen as suitable cysteine positions for labelling. Labelling and surface-immobilization of the proteins did not alter the substrate dissociation constant K_D (Table S2.1). In our assays, the interprobe distance reports on the relative orientation and distance between the subdomains of the SBP and is thus indicative for the degree of closing. The relative interprobe distance can be accessed via the apparent FRET efficiency of freely-diffusing or surface-immobilized protein molecules. Although this approach monitors only a single distance in the SBP, it permits rapid screening of substrate induced conformational changes in physiologically relevant conditions.

The apparent FRET efficiency of individual and freely-diffusing SBPs were measured in the presence and absence of their cognate substrates using confocal microscopy. We observed that at saturating concentrations of cognate substrate, i.e., above the K_D (Table S2.1), the FRET efficiency histograms and the fitted Gaussian distributions are shifted to higher values compared to substrate-free conditions (Figure 2.2B-G; Table S2.2). This

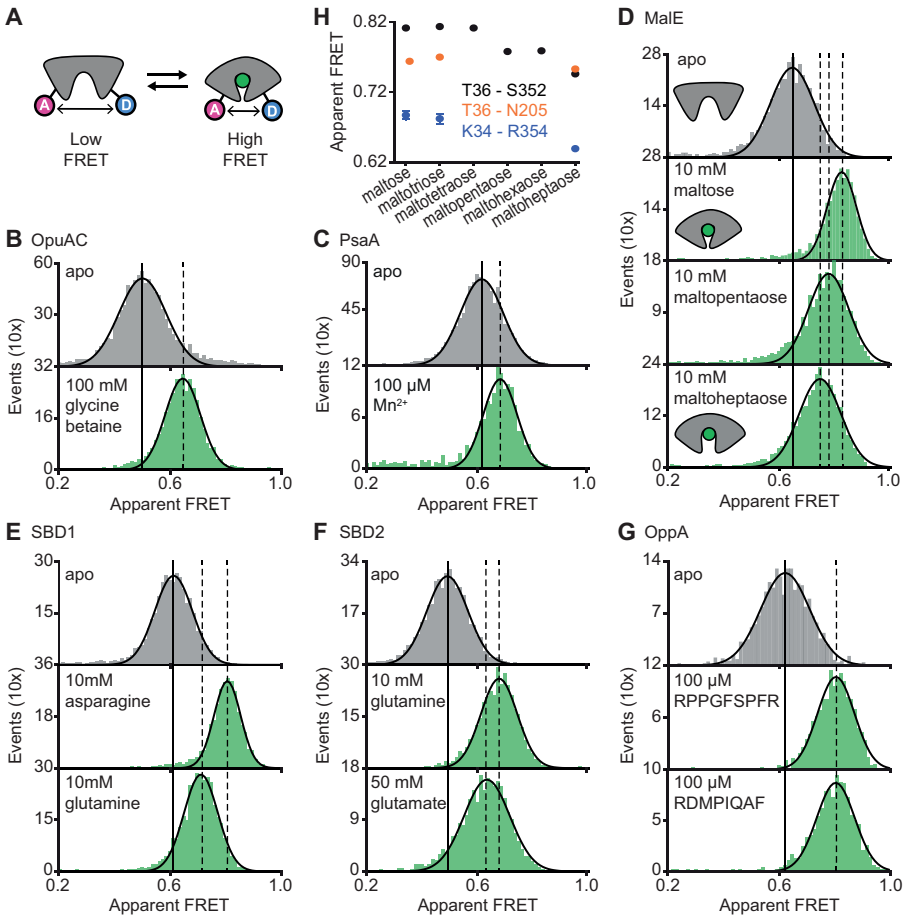

Figure 2.2. Conformational states of SBPs probed by smFRET reveal multiple active conformations. (A) Experimental strategy to study SBP conformational changes via FRET. Solution-based apparent FRET efficiency histograms of OpuAC(V360C/N423C) (B), PsaA(V76C/K237C) (C), MalE(T36C/S352C) (D), SBD1(T159C/G87C) (E), SBD2(T369C/S451) (F) and OppA(A209C/S441C) (G) in the absence (grey bars) and presence of cognate substrate (green bars). The OppA substrates are indicated by one-letter amino acid code. Bars are the data and the solid line a Gaussian fit. The 95% confidence interval of the Gaussian distribution mean is shown in Table S2.2, and the interval center is indicated by a vertical line (solid and dashed). (H) Mean of the Gaussian distribution of MalE labelled at T36/S352 (black), T36/N205 (orange) and K34/R352 (blue). Error bars indicate 95% confidence interval.

indicates a reduced distance between the SBP subdomains and inferred to be closure of the proteins. For individual surface-immobilized SBPs we observed substrate induced opening and closing transitions in the presence of substrate concentrations at the respective K_D value (Figure S2.1). The solution-based FRET distributions of substrate-bound and substrate-free SBPs are unimodal and thus do not reveal any substantial conformational heterogeneity, such

as a pronounced closing in the absence of substrate or a substantial population of the open state when the protein has a substrate bound (Section 2.2.2). This strongly suggests that substrates are bound via an induced-fit mechanism, unless dynamics occurs on timescales faster than milliseconds. This inference was further substantiated by examining individual surface-immobilized OppA proteins and observing that substrate induced SBP closing follows first-order kinetics while the opening obeys zeroth-order kinetics (Figure S2.2)[32].

Further examination of the FRET distributions shows that multiple substrate-bound SBP conformations exist for SBD1, SBD2 and MalE (Figure 2.2D-F). For the amino acid binding proteins SBD1 and SBD2, the cognate substrates[37] asparagine and glutamine for SBD1, and glutamine and glutamate for SBD2 all stabilize a distinct protein conformation, as shown by the FRET efficiency histograms and fitted Gaussian distributions (Figure 2.2E-F; Table S2.2). Notably, closure of SBD1 by asparagine reduces the interprobe distance compared to the substrate-free protein by ~9 Å (Table S2.2). In contrast, glutamine binding reduces the distance by ~5 Å, suggesting that only a partial closing of SBD1 occurs. In SBD2, glutamine and glutamate reduce the distance ~9 and ~7 Å, respectively (Table S2.2).

For the maltodextrin-binding protein MalE we examined the effect of cognate maltodextrins[39], ranging from two to seven glucosyl units, on the protein conformation. Comparison of the FRET efficiency histograms of the different MalE-substrate complexes shows that at least three distinct substrate-bound MalE conformations exist (Figure 2.2D; Figure S2.3A; Table S2.2). In contrast to SBD1 and SBD2, some cognate substrates did not induce a unique MalE conformation (Figure S2.3A). For instance, maltopentaose and maltohexaose elicited the same FRET change, and triggered the formation of a partial closed MalE conformation with a ~7 Å reduction in the interprobe distance. This conformation is different from the fully closed form of MalE, that is formed with maltose, maltotriose and maltotetraose, wherein the interprobe distance is reduced by ~10 Å. Further, it is also distinct from the other partially closed conformation induced by maltoheptaose where the interprobe distance is reduced by ~5 Å. These results were confirmed by examining different labelling positions (Figure 2.2H; Figure S2.4). However, whether this conformational plasticity is a universal feature among SBPs needs to be investigated further, because in OppA the four examined cognate substrates[43] elicited the same FRET change (Figure 2.2G; Figure S2.3B). The findings on the conformational changes (and differences) for each SBP were statistically robust by the non-parametric two-way Kolmogorov-Smirnov (KS) test (data not shown), which indicates the absence of any fitting bias. Thus, these data indicate that although the examined SBPs have a single open conformation, a productive interaction between the SBP and the translocator does not require a single, unique closed SBP conformation. The structural flexibility of the SBP permits the formation of one or more conformations, all of which are able to interact with the translocator and initiate transport[37-40, 43].

2.2.2 Intrinsic conformational changes of SBPs

We then investigated whether the conformational changes in the SBPs that were triggered by their substrates, can also occur in their absence. To address this, we investigated surface-tethered SBPs in the absence of substrate. Compared to the solution-based smFRET experiments, measuring individual surface-tethered SBPs greatly increases the sensitivity to detect rare events. Proteins were immobilized on a glass-coverslip via an anti-his antibody (Figure 2.3A). The positions of the individual proteins were identified by using confocal scanning microscopy (see Materials and Methods). The position information was subsequently used to generate fluorescence trajectories with millisecond temporal resolution. In contrast to other studies[28, 29, 32, 33], the labelled proteins were supplemented with high concentrations of unlabelled protein (10-20 μM), or the divalent chelating compound ethylenediaminetetraacetic acid (1 mM EDTA for PsaA), to remove any potential contaminating substrates (Figure 2.3A). Contaminations could otherwise lead to FRET changes that are misinterpreted as intrinsic closing.

Consistent with the solution-based measurements of Figure 2.2, we observed that all SBPs were predominantly in a low FRET state (open conformation; Figure 2.3B-G; Figure S2.5). For substrate-free MalE, PsaA and OpuAC, no transitions to higher FRET states were observed within a total observation time of at least 8 min for each SBP (Figure 2.3B-D; Table S2.3). In SBD1, SBD2 and OppA rare transitions to a high FRET state were observed and have an average lifetime of 205 ± 36, 90 ± 11 and 211 ± 42 ms (mean ± s.e.m.), respectively (Figure 2.3E-G; Figure S2.5D-F). Transitions towards these states occur only rarely, on average only ~4 times per minute (Figure 2.3H; Table S2.3). To rule out that these infrequent FRET transitions are caused by rare binding events arising from any non-chelated substrate, we recorded an additional data set of fluorescence trajectories for SBD1, SBD2 and OppA in the presence of a 4 to 10-fold lower concentration of unlabelled protein. We observed that in these fluorescence trajectories the FRET transitions occur with a similar frequency and have the same average lifetime compared to when 10-20 μM unlabelled protein was present (Figure S2.6). This suggests that all potential substrate contaminations are efficaciously scavenged by the unlabelled protein, thus providing compelling evidence that the rare FRET transitions observed in SBD1, SBD2 and OppA represent intrinsic closing of the protein. Therefore, some SBPs have the ability to also close without substrate. However, not all SBPs undergo intrinsic conformational transitions, e.g., MalE, PsaA and OpuAC, unless these occur below the temporal resolution of the measurements (millisecond timescale). Overall, the data indicate that diversity exists in the conformational dynamics of substrate-free SBPs.

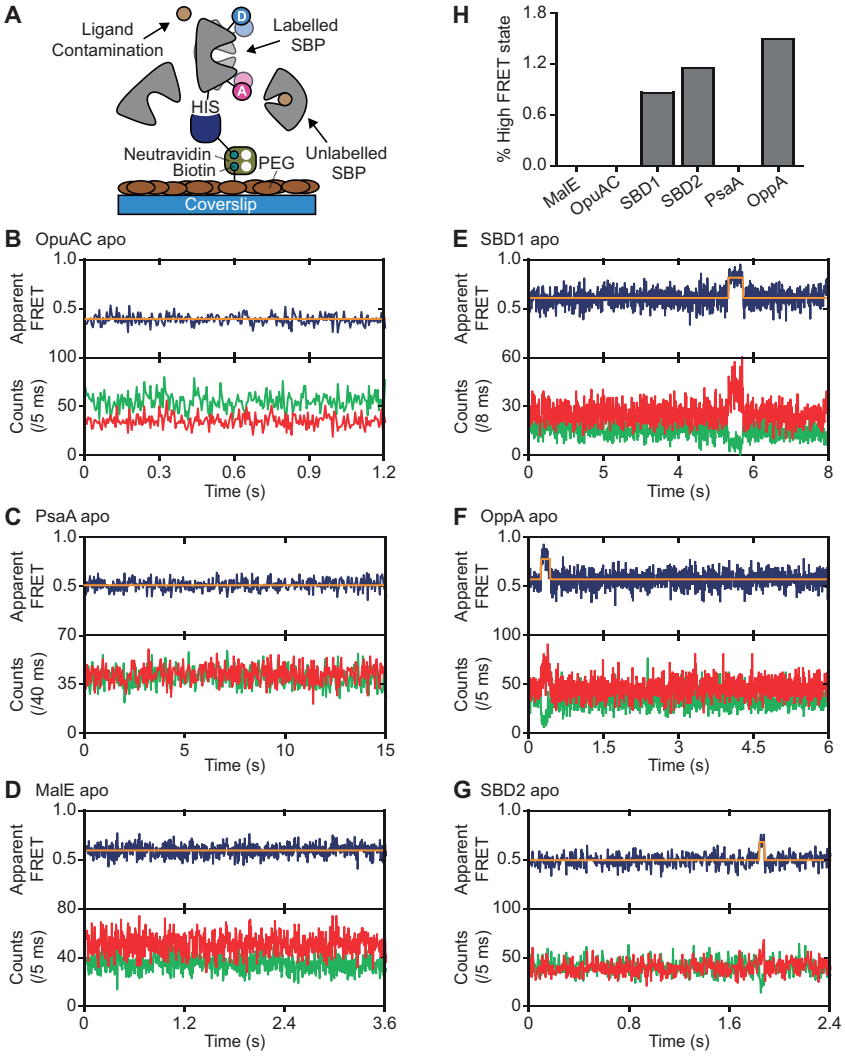

Figure 2.3. Rare conformational states of substrate-free SBPs. (A) Schematic of the experimental strategy to study the conformational dynamics of substrate-free SBPs. Representative fluorescence trajectories of OpuAC(V360C/N423C) (B), PsaA(V76C/K237C) (C), MalE(T36C/S352C) (D), SBD1(T159C/G87C) (E), OppA(A209C/S441C) (F) and SBD2(T369C/S451) (G) in the absence of substrate. 10-20 μM of unlabelled protein or 1 mM EDTA (for PsaA) was added to scavenge any substrate contaminations. In all fluorescence trajectories presented in the figure: top panel shows calculated apparent FRET efficiency (blue) from the donor (green) and acceptor (red) photon counts as shown in the bottom panels. Orange lines indicate average apparent FRET efficiency value or most probable state-trajectory of the Hidden Markov Model (HMM). Statistics can be found in Table S2.3. (H) Percentage of time an SBP is in the high FRET state.

2.2.3 How do non-transported substrates influence the SBP conformation?

Ensemble FRET measurements using all proteinogenic amino acids and citrulline were performed to obtain full insight into the substrate specificity of SBD1 and SBD2 of GlnPQ. Asparagine, glutamine and histidine trigger a FRET change in SBD1, and glutamine in SBD2 (Figure S2.7). Glutamate triggers only a change in SBD2 at low pH, i.e., when a substantial fraction of glutamic acid is present. No other amino acid affected the apparent FRET efficiency. However, arginine and lysine competitively inhibit the conformational changes induced by asparagine binding to SBD1 and glutamine binding to SBD2 (Figure S2.8). Uptake experiments in whole cells and in proteoliposomes show that histidine, lysine and arginine are not transported by GlnPQ, but these amino acids can inhibit the uptake of glutamine (via SBD1 and SBD2) and asparagine (via SBD1) (Figure 2.4A-C). Thus, some amino acids interact with the SBPs of GlnPQ but fail to trigger transport. Similar substrates have been identified for MalE, OpuAC and PsaA[16, 38-40], and we refer to these as non-cognate substrates. We then used smFRET to test whether or not substrate induced SBP conformational changes allow discriminating cognate from non-cognate substrates.

We observed that at saturating concentrations of most non-cognate substrates the FRET efficiencies are altered compared to the substrate-free conditions (Figure 2.4D-H; Table S2.2). This shows that, similar to cognate substrates (Figure 2.3B-G), non-cognate substrate binding is coupled to SBP conformational changes. However, this is not true in all cases, as the binding of the non-cognate substrates arginine and lysine in SBD1 and arginine in SBD2 do not alter the FRET efficiency histograms (Figure 2.4D-E), suggesting that these substrates bind in the open conformation of the SBP and do not trigger a conformational change.

Further analysis of the non-cognate substrate induced conformational changes reveals states that vary, from larger opening (carnitine-OpuAC in Figure 2.4G), to partial closing (histidine-SBD1 in Figure 2.4D; various maltodextrin-MalE complexes in Figure 2.4F; proline-OpuAC in Figure 2.4G) or full closing (Zn^{2+}-PsaA in Figure 2.4H) of the SBP relative to the substrate-free state of the corresponding protein. The data of full closing by Zn^{2+} (non-cognate) and Mn^{2+} (cognate) were confirmed by examining different labelling positions in PsaA (Figure S2.9) and are in line with prior crystallographic analyses[40, 50]. Noteworthy, the non-cognate substrate histidine and the cognate substrate glutamine induce both partial closing of SBD1 (Figure 2.4D). However, histidine elicited a larger FRET shift in SBD1 (~7 Å reduction in interprobe distance) than cognate glutamine (~5 Å), but smaller than the cognate substrate asparagine (~9 Å), which induced full closing (Figure 2.4D; Table S2.2). In contrast, the FRET shift induced with certain non-cognate substrates in MalE (β-cyclodextrin, maltotriitol and maltotetraitol) and OpuAC (proline) are smaller, and

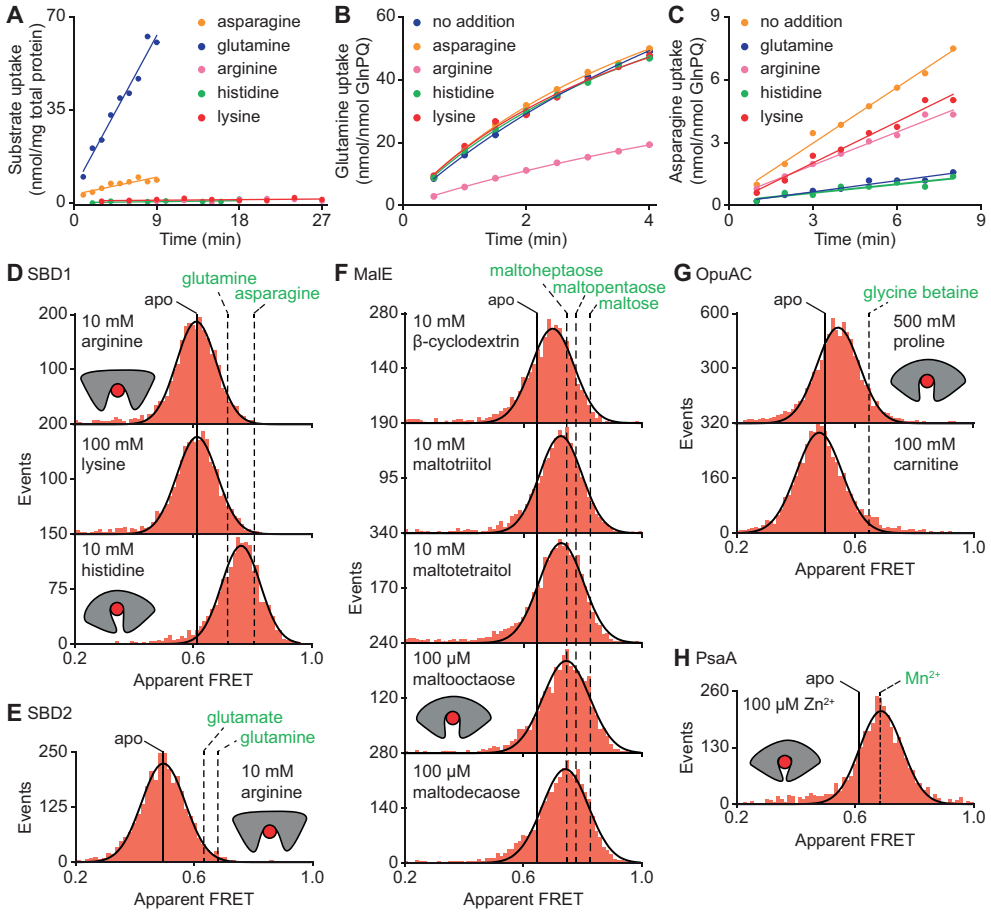

Figure 2.4. Substrate specificity of GlnPQ and SBP conformations with non-cognate substrates. (A) Time-dependent uptake of [^{14}C]-asparagine (5 µM), [^{14}C]-glutamine (5 µM), [^{14}C]-arginine (100 µM), [^{14}C]-histidine (100 µM) and [^{3}H]-lysine (100 µM) by GlnPQ in *L. lactis* GKW9000 complemented *in trans* with a plasmid for expressing GlnPQ. Points are the data and the solid line a hyperbolic fit. Time-dependent uptake of glutamine (B) and asparagine (C) in proteoliposomes reconstituted with purified GlnPQ (see Materials and Methods). The final concentration of [^{14}C]-glutamine and [^{14}C]-asparagine was 5 µM; the amino acids indicated in the panel were added at a concentration of 5 mM. Solution-based apparent FRET efficiency histogram of SBD1(T159C/G87C) (D), SBD2(T369C/S451) (E), MalE(T36C/S352C) (F), OpuAC(V360C/N423C) (G) and PsaA(V76C/K237C) (H) in the presence of non-cognate (red bars) substrates as indicated. Bars are the data and solid line a Gaussian fit. The 95% confidence interval for the distribution mean is shown in Table S2.2. The interval center is indicated by a vertical line (solid and dashed).

correspond to a reduction in the interprobe distance of ~3-4 Å, than with their cognate substrates, which reduce the interprobe distance ~5-10 Å (Figure 2.4F-G; Table S2.2). Intriguingly, the data also suggest that the partially closed SBP-substrate complexes of MalE formed with the non-cognate substrates maltooctaose or maltodecaose are similar to that of

the cognate substrate maltoheptaose (Figure 2.4F). Again, this result was confirmed by examining different labelling positions (Table S2.2). The findings on the conformational changes for each SBP were statistically robust by the two-way KS test.

In summary, similar to cognate substrates, non-cognate substrates do not induce a single unique substrate-bound SBP state, and solely from the degree of SBP closing a translocator cannot readily discriminate cognate from non-cognates substrates. Notable exceptions are the substrates that do not induce closing and keep the SBP in the open state. This raises fundamental questions as to the mechanistic basis for how certain non-cognate substrates are still excluded from import.

2.2.4 Altered SBP opening renders PsaA permissive for Zn^{2+} transport

The inability of certain substrates to be transported, while they appear to induce SBP conformations that are similar to those associated with cognate substrates, was observed for MalE (Figure 2.4F) and PsaA (Figure 2.4H). First, this was investigated further for PsaA. Upon addition of 1 mM EDTA to PsaA-Mn^{2+}, lower FRET efficiencies are instantaneously recorded (Figure 2.5A), indicating that the lifetime of the closed PsaA-Mn^{2+} conformation is shorter than a few seconds. By contrast, Zn^{2+} kept PsaA closed, irrespective of the duration of the EDTA treatment (up to 15 min) (Figure 2.5B). Irreversible and reversible binding of these metals was shown previously[51], which can now be explained by the extremely slow and fast opening of PsaA in the presence of Zn^{2+} and Mn^{2+}, respectively. The extremely slow opening of PsaA may explain why Zn^{2+} is not transported by PsaBCA, as opening of the SBP is required for release of the substrate to the translocator. However, it is also possible that the translocator controls the transport specificity[20, 21]. To discriminate between these two scenarios, we examined the impact of altered SBP dynamics on the transport activity of PsaBC. We substituted an aspartate in the binding site with asparagine (D280N), which has previously been shown to perturb the stability of the Zn^{2+}-bound SBP[51]. Analysis of PsaA and PsaA(D280N), at saturating Zn^{2+} concentrations, revealed similar FRET efficiency histograms for the two proteins (Figure 2.5C; Table S2.2). However, in contrast to the Zn^{2+}-PsaA complex, opening of the PsaA(D280N) complex renders Zn^{2+} accessible to EDTA, similar to the cognate substrate Mn^{2+} (Figure 2.5A, C). The ability of PsaA(D280N) to open and release Zn^{2+} was then assessed by measuring the cellular accumulation of Zn^{2+} within *Streptococcus pneumoniae*, the host organism. This was achieved by replacement of the *psaA* gene with the D280N mutant allele ($\Omega psaA_{D280N}$) in a strain permissive for Zn^{2+} accumulation, i.e., incapable of Zn^{2+} efflux due to deletion of the exporter CzcD ($\Omega psaA_{D280N}\Delta czcD$)[52]. Our data show that cellular Zn^{2+} accumulation increases in the strain expressing PsaBC with PsaA(D280N) but not with PsaA (Figure 2.5D). These results show

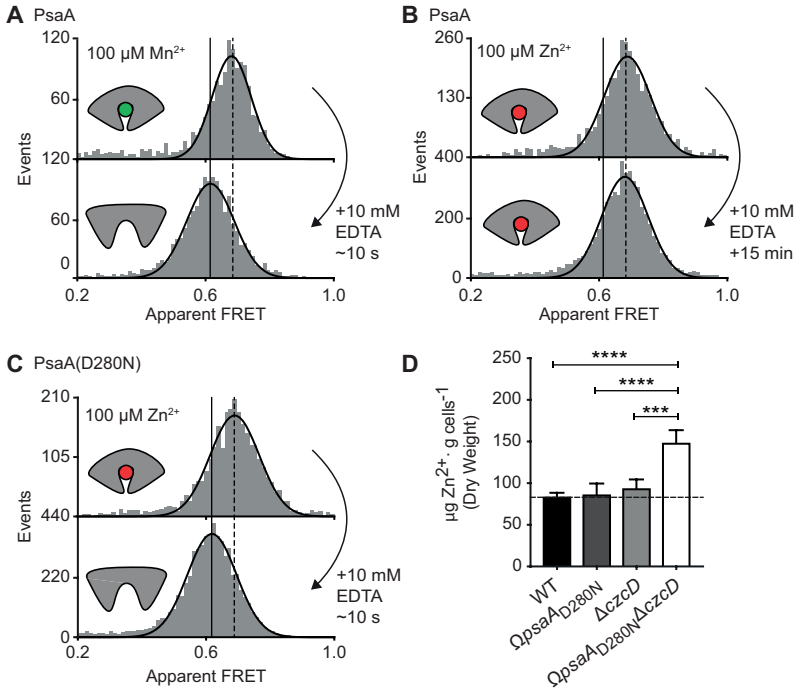

Figure 2.5. Opening transition in PsaA dictates transport specificity. Solution-based apparent FRET efficiency histograms of PsaA(V76C/K237C) in the presence of Mn^{2+} (A) or Zn^{2+} (B) and PsaA(D280N) in the presence of Zn^{2+} (C) upon addition of 10 mM EDTA and incubated for the indicated duration. Bars are the data and the solid line a Gaussian fit. The 95% confidence interval for the mean of the Gaussian distribution can be found in Table S2.2, and the interval center is indicated by vertical lines (solid, metal-free and dashed, metal-bound). (D) Zn^{2+} accumulation in *S. pneumoniae* D39 and mutant strains in CDM supplemented with 50 μM $ZnSO_4$ as determined by ICP-MS. Data correspond to mean ± s.d. μg $Zn^{2+}\cdot g^{-1}$ dry cell weight from three independent biological experiments. Statistical significance was determined by one-way analysis of variance with Tukey post-test (***p<0.005 and ****p<0.0001).

that the altered conformational dynamics of the PsaA derivative renders substrate release permissive for transport of Zn^{2+} ions. The data also show that translocator activity is not directly influenced by the nature of the metal ion released by PsaA. Collectively, our findings demonstrate that transport specificity of PsaBCA is dictated by the opening kinetics of PsaA.

2.2.5 MalE conformational dynamics with cognate and non-cognate substrates

Next, we determined the conformational dynamics of MalE induced by maltoheptaose, maltooctaose and maltodecaose. Similar to Zn^{2+} and Mn^{2+} in PsaA (Figure 2.4H), these substrates appear to induce similar MalE conformations (Figure 2.4F) but only maltoheptaose is transported[39]. Measurements on individual surface-tethered MalE proteins, in the presence of maltoheptaose, maltooctaose or maltodecaose, show frequent switching

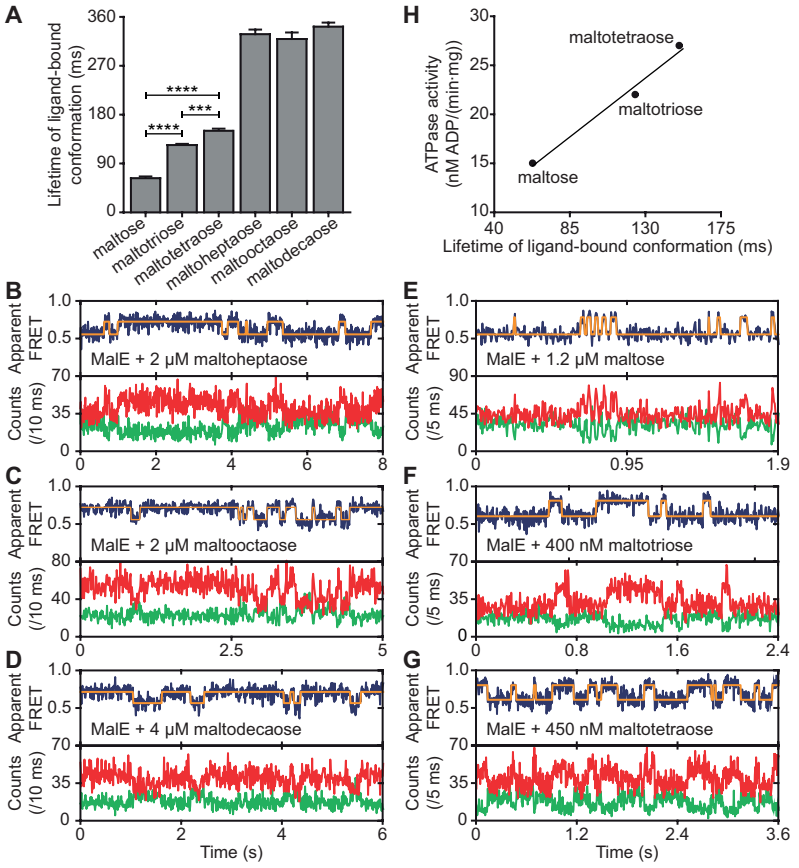

Figure 2.6. Lifetime of MalE substrate-bound conformations and relation to activity. (A) Mean lifetime of the substrate-bound conformations of MalE, obtained from all single-molecule fluorescence trajectories in the presence of different maltodextrins as indicated. Data corresponds to mean ± s.e.m.. Statistical significance was determined by the two-tailed unpaired *t*-tests (***p<0.005 and ****p<0.0001). (B-G) Representative fluorescence trajectories of MalE(T36C/S352C) in the presence of different cognate substrates as indicated. In all fluorescence trajectories presented: top panel shows calculated apparent FRET efficiency (blue) from the donor (green) and acceptor (red) photon counts as shown in the bottom panels. Most probable state-trajectory of the HMM is shown (orange). (H) Published ATPase activity[16] versus the lifetime of the closed conformation as function of different cognate substrates as indicated. Points are the data and the solid line a simple linear regression fit.

between low and higher FRET states, corresponding to opening and (partial) closing of MalE (Figure 2.6A-D). Consistent with the solution-based smFRET measurements, the average apparent FRET efficiency of the high FRET state is similar for these maltodextrins and lower than with maltose (Figure S2.10). The mean lifetime of the substrate-bound conformations, i.e., the mean lifetime of the high FRET states, are 328 ± 8 ms for cognate maltoheptaose and 319 ± 12 ms and 341 ± 8 ms for non-cognate maltooctaose and maltodecaose, respectively (mean ± s.e.m.; Figure 2.6A, Figure S2.11). So, contrary to PsaA-Zn^{2+}, a slow

opening of MalE and inefficient substrate release kinetics cannot explain why maltooctaose and maltodecaose are not transported; the average lifetimes with maltooctaose or maltodecaose are not significantly different from that with maltoheptaose (p=0.68, one-way analysis of variance; Figure 2.6A). Most likely, the failure of the maltose importer to transport maltooctaose and maltodecaose originates in the size limitations of the translocator domain of $MalFGK_2$[20].

2.2.6 Translocator/SBP interplay determines the rate of transport

Finally, we sought to elucidate the mechanistic basis for how substrate preference arises in the maltose system and to what degree the translocator contributes to this process. First, we investigated how the MalE conformational dynamics influences the transport rate of the substrate maltose. For this we used the hinge-mutant variant MalE(A96W/I329W) that has different conformational dynamics compared to the wild type MalE protein (Figure 2.6E; Figure S2.12A-B)[32]. The mutations are believed to not affect SBP-translocator interactions since they are situated on the opposite side of the interaction surface of the SBP[44, 53].

At saturating concentrations of maltose the FRET efficiency distributions of MalE and MalE(A96W/I329W) are indistinguishable (Figure S2.12C). This could be confirmed by two different interprobe positions in each protein. Therefore, changes in the rate of maltose transport unlikely arise from differences in SBP docking onto the TMD, since similar SBP conformations are involved. Nonetheless, cellular growth and the maltose-induced ATPase activity are reduced for MalE(A96W/I329W)[53, 54]. Analysis of the mean lifetime of the closed conformation of MalE(A96W/I329W) shows that the opening of the protein is almost three orders of magnitude slower than in the wild type protein (63 ± 6 ms (mean ± s.e.m.) in MalE versus 28 ± 5 s (mean ± s.e.m.) in MalE(A96W/I329W); Figure 2.6A; Figure S2.12B). These observations suggest that the maltose-stimulated cellular growth and ATPase activity are reduced due to the slower substrate release of MalE(A96W/I329W) compared to wild type MalE. This negative correlation between the MalE lifetime and the transport activity is in line with the observation that Zn^{2+}-PsaA(D280N) opens fast, so that Zn^{2+} transfer to the translocator and import can occur, whereas in wild type Zn^{2+}-PsaA the opening is (extremely) slow and import does not occur (Figure 2.5).

We then investigated the relationship between maltodextrin-specific lifetimes of the MalE closed conformations and published transport rates or ATPase activities of the full transport system[16]. Here, we focused on the cognate substrates maltose, maltotriose and maltotetraose. Analysis of individual surface-tethered MalE proteins in the presence of these substrates shows that the average lifetime of the closed conformation with maltose, maltotriose and maltotetraose are 63 ± 6, 124 ± 4, and 150 ± 8 ms (mean ± s.e.m.),

respectively (Figure 2.6A; Figure 2.6E-G; Figure S2.11). Thus, these lifetimes correlate positively with their stimulation of the ATPase activity (Figure 2.6H)[16]. A positive relationship also exists between the lifetimes with maltose and maltotetraose (63 ± 6 and 150 ± 8 ms, respectively) and their corresponding transport rates (transport of maltotetraose is ~1.5-fold faster than of maltose)[16]. This positive correlation is inconsistent with our earlier findings that a shorter SBP lifetime results in a faster rate of transport. However, this relationship only holds when the SBP conformational dynamics are altered, while leaving all other rate-determining steps of the transport process unaffected. Thus, the observation that some maltodextrins induce a faster opening of MalE, while their corresponding transport and/or stimulation of ATP hydrolysis are slower, implies that the kinetics of certain other rate-determining steps are substrate-dependent. Faster transport or ATP hydrolysis can arise when certain maltodextrins trigger these steps more efficiently than others, thereby overcoming the slower opening of MalE. These steps most likely occur after opening of MalE, as these differences in transport activity are unlikely to arise from differences in docking of MalE onto the TMDs (crystallographic[15] and smFRET data (Table S2.2) shows that maltose, maltotriose and maltotetraose induce similar MalE conformations) or arise from differences in the binding affinity of MalE[16]. Thus, although the precise molecular mechanism of the rate-determining steps remains elusive, the positive correlation between lifetime of the SBP closed conformation and the activity of the transporter strongly suggests involvement of the translocator $MalFGK_2$ in influencing the transport rate of certain maltodextrins.

2.3 Discussion

Prokaryotes occupy diverse ecological niches within terrestrial ecosystems. Irrespective of the niche, their viability depends on selective acquisition of nutrients from the extracellular environment. However, the diversity of the external milieu poses a fundamental challenge for how acquisition of specific compounds can be achieved within the constraints of the chemical selectivity conferred by their import pathways. Numerous studies on SBPs of ABC importers have established that these proteins share a common architecture, contain a high affinity substrate-binding site and form a distinct apo and holo conformation, i.e., open and closed[2, 7, 8]. Building on this knowledge, we investigated the relationship between SBP conformational dynamics, SBP-substrate interactions and transport.

The general view of SBP conformational changes serving as a binary switch to communicate transport competency may hold for some SBPs, such as OppA, while others employ multiple distinct substrate-bound conformations (Figures 2.2 and 2.4). To our knowledge, such extreme conformational plasticity of SBPs has not been observed before.

MalE shows a remarkable structural flexibility of at least five different substrate-bound conformations (Figure 2.2D; Figure 2.4F). SBD1 can sample at least four distinct substrate-bound conformations and SBD2 and OpuAC at least three (Figures 2.2 and 2.4). Moreover, MalE, SBD1 and SBD2 have multiple distinct substrate-bound conformations that can all interact with the translocator, as they all facilitate substrate import ('multiple conformations activate transport' in Figure 2.7; Figure 2.2D-F). Thus, a productive SBP-translocator interaction in Type I ABC importers can be accomplished without relying on strict structural requirements for docking. This generalization may not apply to all Type I ABC importers since in the Opp importer the translocator might only interact with a unique closed conformation of the SBP OppA (Figure S2.3B), and Opp has no measurable affinity for its open substrate-free conformation[46].

Exclusion of non-cognate substrates is also a critical biological function for SBPs. Our work has uncovered a hitherto unappreciated complexity in protein-substrate interactions and how this is coupled to the regulation of substrate import. Similar to transport, exclusion of non-cognate substrates might be achieved by multiple distinct mechanisms. We have shown that although multiple SBP conformations can activate transport (Figure 2.2), not all SBP conformational states appear to provide the signal to facilitate transport. For example, the binding of certain non-cognate substrates induces a conformational change in SBD1, MalE and OpuAC that are distinct from those that facilitate transport (Figure 2.4). However, non-cognate substrate binding is not always coupled to an SBP conformational change, as observed for the binding of arginine or lysine to SBD1 and arginine to SBD2 (Figure 2.4D-E). These observations provide a general explanation on how substrate import can fail in Type I ABC importers, which would be due to the SBP-substrate complex assuming a conformation that cannot initiate allosteric interactions with the translocator ('conformational mismatch' in Figure 2.7). A similar hypothesis was put forward based on the observation that binding of β-cyclodextrin fails to fully close MalE[17-19]. However, the sole observation of partial closing of MalE cannot explain why transport of β-cyclodextrin fails, as we here show that also cognate maltodextrins are able to induce partial closing of MalE (Figure 2.2D).

In contrast, in the Mn^{2+} transporter PsaBCA, a different mechanism is used. In PsaA, the binding site composition of the SBP precludes the ability of the protein to exclude the non-cognate substrate Zn^{2+} from interacting. As a consequence, both metals bind and trigger formation of similar PsaA conformations ('conformational match' in Figure 2.7; Figure 2.4H)[40, 50]. Despite this, the two ions induce starkly different conformational dynamics of PsaA, with Zn^{2+} forming a highly stable closed conformation, such that it cannot open and release the substrate to its translocator ('SBP cannot open' in Figure 2.7; Figure 2.5). By altering the binding site interactions between PsaA and Zn^{2+}, opening is faster

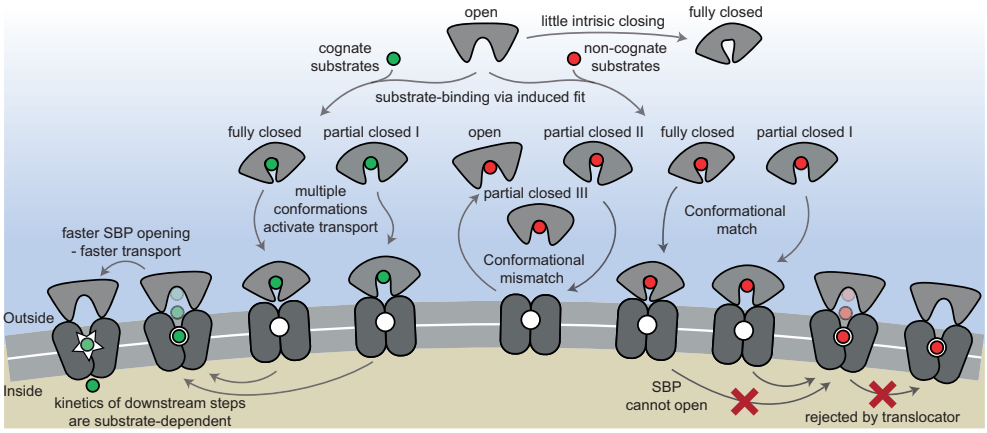

Figure 2.7. The conformational changes and dynamics of SBPs and transport function. Schematic summarizing the plasticity of substrate binding and solute import via ABC importers. Intrinsic closing of an SBP is a rare event or absent in some SBPs ('little intrinsic closing'). Substrates are bound via the induced-fit mechanism ('substrate-binding via induced fit'). SBPs can acquire one or more conformations that can activate transport ('multiple conformations activate transport'). Variations in cognate substrate transport are caused by: (i) openings rate of the SBP and substrate transfer to the translocator ('faster SBP opening – faster transport') and (ii) substrate-dependent downstream steps ('kinetics of downstream steps are substrate-dependent'). Although some SBPs form a conformation that could activate transport ('conformational match'), transport still fails when: (i) the SBP cannot open and release the substrate to the translocator ('SBP cannot open') or (ii) due to the specificity and size limitations of the translocator ('rejected by translocator'). Transport could also fail when the SBP has no affinity for the translocator and/or cannot make the allosteric interaction with the translocator ('conformational mismatch').

and transport of the metal ion can occur (Figure 2.5). Similar observations were made for GlnPQ[29, 55] and MalE (Figure 2.6E; Figure S2.12A), in which a slower opening of the SBP resulted in a lower transport rate and ATP hydrolysis rate ('faster SBP opening – faster transport' in Figure 2.7). We therefore conclude that for substrates that induce highly stabilized SBP-substrate conformations, which require more energy (thermal or ATP-dependent) to open, transport becomes slower or is abrogated. Based on these findings, we infer that biological selectivity in ABC importers is largely achieved via a combination of substrate release kinetics and its influence on the conformational state of the SBP. This provides a mechanism to facilitate the import of selective substrates, while excluding other compounds. However, our data also implicate a role for the translocator in contributing to the specificity of ABC importers ('rejected by translocator' in Figure 2.7), consistent with previous studies[20, 21, 48, 56].

The presence of a substrate-binding site in the translocator of the maltose system is well-established[20, 48], although its role, if any, in influencing the rate of transport of maltodextrins is yet unknown. We observed that the average time required for the different maltodextrin-MalE complexes to open and release the substrate, correlates positively with the transport

and ATP hydrolysis rate (Figure 2.6H)[16]. This suggests that the substrate, after it has been transferred from MalE to the translocator, acts as a trigger for subsequent steps, for example, the transition from the outward- to the inward-facing transporter conformation or the stimulation of ATP hydrolysis and/or P_i and ADP release ('kinetics of downstream steps are substrate-dependent' in Figure 2.7). Irrespective of the precise molecular mechanism, the positive correlation between the lifetime of the SBP closed state and activity of the transporter implies that some maltodextrins trigger certain steps more efficient than other maltodextrins, thereby overcoming the slower opening of MalE, and leading to a preferred uptake of certain maltodextrins over others. When transport is solely altered by changing the SBP conformational dynamics, for example in MalE(I329W/A96W) and PsaA(D280N), the kinetics of these steps remains unaltered, as the same substrates are involved, thus explaining the observed negative correlation between the lifetime of the SBP and transport in these specific cases.

The volume of the binding cavities in the translocator could be a limiting factor for transport via ABC importers. Analysis of the large non-cognate substrates maltooctaose and maltodecaose shows that these are bound reversibly by MalE (Figure 2.6A) and induce MalE conformations similar to that of the cognate substrate maltoheptaose ('conformational match' in Figure 2.7; Figure 2.4F). Therefore, failure of the maltose system to transport maltooctaose and maltodecaose most likely arises due to size limitations of the translocator rather than failure of MalE to close and release the bound substrate. This supposition is supported by an analysis of the binding cavities in the crystal structure of $MalFGK_2$-MalE[20]. These data suggest that the transporter could only accommodate maltodextrins as large as maltoheptoase. In contrast, MalE could accommodate larger maltodextrins, including β-cyclodextrin (Figure 2.4F), probably due to its greater structural flexibility (Figure 2.2D; Figure 2.4F), thereby allowing the binding pocket to adapt and substrates to extend into the solvent phase.

The presence of two consecutive binding pockets, one in the SBP and one in the translocator, in at least some ABC importers could indicate that specificity of transport occurs through a proofreading mechanism in a manner analogous to aminoacyl-tRNA synthetases and DNA polymerase[57, 58]. In such a mechanism, a substrate can be rejected even if it has been bound by the SBP. Although we show that intrinsic closing is a rare event ('little intrinsic closing' in Figure 2.7; Figure 2.3), it might influence transport in a cellular context where the ratio between SBP and translocator can be high[59]. Moreover, other fast (μs-ms) and short-range conformational changes might be present as shown by NMR analysis on MalE[27]. We speculate that in Type I ABC importers the wasteful conversion of chemical energy is prevented by a proofreading mechanism, as any thermally driven closing event would not be able to initiate the translocation cycle, as the substrate is absent. In accordance,

ATP hydrolysis and transport are tightly coupled in the Type I importer GlnPQ[60] that, based on the crystal structure of the homologous Art(QM)$_2$[21], contains an internal binding pocket located within the TMDs. By contrast, high futile hydrolysis of ATP in the Type II BtuCDF[61] appears to correlate with the lack of a defined binding pocket inside the TMDs.

2.4 Materials and Methods

Gene expression and SBP purification. N-terminal extension of the soluble SBPs with a His$_x$tag (His$_{10}$PsaA, His$_{10}$SBD1, His$_{10}$SBD2, His$_{10}$OppA and His$_6$OpuAC) were expressed and purified as previously described[29, 38, 43, 51]. Protein derivatives having the cysteine point mutations were constructed using QuickChange mutagenesis[62] or Megaprimer PCR mutagenesis[63] protocols. OppA, OpuAC, PsaA and PsaA(D280N) derivatives were constructed using as templates the vectors pNZcLIC-OppA[64], pNZOpuCHis[65], pCAMcLIC01-PsaA[51] and pCAMcLIC01-PsaAD280N[51], respectively. Construction of SBD1 and SBD2 cysteine derivatives was accomplished as described previously[29]. The *malE* gene (UniProt: P0AEX9) was isolated from the genome of *Escherichia coli* K12. The primers were designed to exclude the signal peptide (amino acids 1-26). Primers introduced *Nde*I and *Hind*III restriction sites, and the gene product was sub-cloned in the pET20b vector (Merck). MalE derivatives having the cysteine or other point mutations were constructed using QuickChange mutagenesis[62] and Megaprimer PCR mutagenesis[63] protocols. All sequences were checked for correctness by sequencing. His$_6$MalE was over-expressed in *E. coli* BL21 DE3 cells. Cells harbouring plasmids expressing the MalE wild type and derivatives were grown at 30 ºC until an optical density (OD_{600}) of 0.5 was reached. Protein expression was then induced by addition of 0.25 mM isopropyl β-D-1-thiogalactopyranoside (IPTG). After 2 h induction cells were harvested. DNase 500 ug/ml (Merck) was added and passed twice through a French pressure cell at 1,500 psi and 2mM phenylmethylsulfonyl fluoride (PMSF) was added to inhibit proteases. The soluble supernatant was isolated by centrifugation at 50,000×*g* for 30 min at 4 ºC. The soluble material was then purified and loaded on Ni^{2+}-Sepharose resin (GE Healthcare) in 50 mM Tris-HCl, pH 8.0, 1 M KCl, 10% glycerol, 10 mM imidazole and 1 mM dithiothreitol (DTT). The immobilized proteins were washed (50 mM Tris-HCl, pH 8.0, 50 mM KCl, 10% glycerol, 10 mM imidazole and 1 mM DTT plus 50 mM Tris-HCl, pH 8.0, 1 M KCl, 10% glycerol, 30 mM imidazole and 1 mM DTT sequentially) and then eluted (50 mM Tris-HCl, pH 8.0, 50 mM KCl, 10% glycerol, 300 mM imidazole and 1 mM DTT). Protein fractions were pooled (with 5 mM EDTA and 10 mM DTT), concentrated (10.000 MWCO Amicon; Merck-Millipore), dialyzed against 100-1000 volumes of buffer (50 mM Tris-HCl, pH 8.0, 50 mM KCl, 50% glycerol and 10 mM DTT) and stored at -20 ºC.

Uptake experiments of GlnPQ in whole cells. *L. lactis* GKW9000 carrying pNZglnPQhis[66] was cultivated semi-anaerobically at 30 ºC in M17 (Oxoid) medium supplemented with 1% (w/v) glucose and 5 μg/ml chloramphenicol. For uptake experiments cells were grown in GM17 to an OD_{600} of 0.4, induced for 1 h with 0.01% of culture supernatant of the nisin A-producing strain NZ9700 and harvested by centrifugation for 10 min at 4000×*g*; the final nisin A concentration is ~1 ng/ml. After washing twice with 10 mM PIPES-KOH, 80 mM KCl, pH 6.0, the cells were resuspended to OD_{600} of 0.5 in the same buffer. Uptake experiments were performed at 0.1–0.5 mg/ml total protein in 30 mM PIPES-KOH, 30 mM MES-KOH, 30 mM HEPES-KOH (pH 6.0). Before starting the transport assays, the cells were equilibrated and energized at 30 °C for 3 min in the presence of 10 mM glucose plus 5 mM $MgCl_2$. After 3 min, the uptake reaction was started by addition of either [^{14}C]-glutamine, [^{14}C]-histidine, [^{14}C]-lysine (all from PerkinElmer), [^{14}C]-arginine (Moravek) or [^{3}H]-asparagine (ARC); the specific radioactivity was adjusted for each experiment (amino acid concentration) to obtain sufficient signal above background; the final amino acid concentrations are indicated in the figure legends. At given time intervals, samples were taken and diluted into 2 ml ice-cold 100 mM LiCl. The samples were rapidly filtered through 0.45 μm pore-size cellulose nitrate filters (Amersham) and the filter was washed once with ice-cold 100 mM LiCl. The radioactivity on the filters was determined by liquid scintillation counting.

Purification and membrane reconstitution of GlnPQ for in vitro transport assays. Membrane vesicles of *L. lactis* GKW9000 carrying pNZglnPQhis[66] were prepared as described before[60]. For reconstitution into proteoliposomes, 150 mg of total protein in membrane vesicles was solubilized in 50 mM KPi, pH 8.0, 200 mM NaCl, 20% glycerol and 0.5% (w/v) DDM for 30 min at 4 °C. The sample was centrifuged (12 min, 300,00×*g*) and the supernatant was collected. Subsequently, GlnPQ was allowed to bind to Ni^{2+}-Sepharose resin for 1 h at 4 °C after addition of 10 mM imidazole. The resin was rinsed with 20 column volumes of wash buffer (50 mM KPi, pH 8.0, 200 mM NaCl, 20% glycerol, 50 mM imidazole and 0.02% (w/v) DDM). The protein was eluted with 5 column volumes of elution buffer (50 mM KPi, pH 8.0, 200 mM NaCl, 10% glycerol, 500 mM imidazole and 0.02% (w/v) DDM). The purified GlnPQ was used for reconstitution into liposomes composed of egg yolk L-α-phosphatidylcholine and purified *E. coli* lipids (Avanti polar lipids) in a 1:3 ratio (w/w) as described before[67] with a final protein/lipid ratio of 1:100 (w/w). An ATP regenerating system, consisting of 50 mM KPi, pH 7.0, creatine kinase (2.4 mg/ml), Na_2-ATP (10 mM), $MgSO_4$ (10 mM) and Na_2-creatine-phosphate (24 mM) was enclosed in the proteoliposomes by two freeze/thaw cycles, after which the vesicles were stored at -80 °C. On the day of the uptake experiment, the proteoliposomes were extruded 13 times through a polycarbonate

filter (200-nm pore size), diluted to 3 ml with 100 mM KPi, pH 7.0, centrifuged (265,000×g for 20 min), and then washed and resuspended in 100 mM KPi, pH 7.0, to a concentration of 50 mg of lipid/ml. Uptake in proteoliposomes was measured in 100 mM KPi, pH 7.0, supplemented with 5 µM of [^{14}C]-glutamine or [^{3}H]-asparagine. This medium, supplemented with or without unlabelled amino acids (asparagine, arginine, glutamine, histidine or lysine), was incubated at 30 °C for 2 min prior to adding proteoliposomes (kept on ice) to a final concentration of 1-5 mg of lipid/ml. At given time intervals, 40 µl samples were taken and diluted with 2 ml of ice-cold isotonic buffer (100 mM KPi, pH 7.0). The samples were collected on 0.45 µm pore size cellulose nitrate filters and washed twice as described above. After addition of 2 ml Ultima Gold scintillation liquid (PerkinElmer), radioactivity was measured on a Tri-Carb 2800TR (PerkinElmer). A single time-dependent uptake experiment is shown in Figure 2.4A-C and consistent results were obtained upon repetition with an independent sample preparation.

Zinc accumulation in whole cells. The *S. pneumoniae* D39 mutant strains Ω*psaA*$_{D280N}$ and Δ*czcD* were constructed using the Janus cassette system[68]. Briefly, the upstream and downstream flanking regions of *psaA* and *czcD* were amplified using primers with complementarity to either *psaA*$_{D280N}$ (Ω*psaA*$_{D280N}$), generated via site-directed mutagenesis of *psaA* following manufacturer instructions (Agilent), or the Janus cassette (Δ*czcD*) and were joined by overlap extension PCR. These linear fragments were used to replace by homologous recombination *psaA* and *czcD,* respectively, in the chromosome of wild type and Δ*czcD* strains. For metal accumulation analyses, *S. pneumoniae* strains were grown in a cation-defined semi-synthetic medium (CDM) with casein hydrolysate and 0.5% yeast extract, as described previously[69]. Whole cell metal ion accumulation was determined by inductively coupled plasma-mass spectrometry (ICP-MS) as previously described[52]. Briefly, *S. pneumoniae* strains were inoculated into CDM supplemented with 50 µM $ZnSO_4$ at a starting OD_{600} of 0.05 and grown to mid-log phase (OD_{600} of 0.3-0.4) at 37 ºC in the presence of 5% CO_2 . Cells were washed by centrifugation 6 times in PBS with 5 mM EDTA, harvested, and desiccated at 95 ºC for 18 h. Metal ion content was released by treatment with 500 µl of 35% HNO_3 at 95 ºC for 1 h. Metal content was analysed on an Agilent 8900 QQQ ICP-MS[51].

Isothermal titration calorimetry. Purified OppA was dialyzed overnight against 50 mM Tris-HCl, pH 7.4 and 50 mM KCl. Isothermal titration calorimetry experiments were carried out on an ITC200 calorimeter (MicroCal). The peptide (RPPGFSFR) stock solution (200 µM) was prepared in the dialysis buffer and was stepwise injected (2 µl) into the

reaction cell containing 20 µM OppA. All experiments were carried out at 25 ºC with a mixing rate of 400 rpm. Data were analysed with a one site-binding model.

Ensemble FRET. Fluorescence spectra of labelled SBD1 and SBD2 proteins were measured on a scanning spectrofluorometer (Jasco FP-8300; λ_{ex} = 552 nm, 5 nm excitation and emission bandwidth; 3 s integration time). The apparent FRET efficiency was calculated via $I_{Acceptor}/(I_{Acceptor}+ I_{donor})$, where $I_{Acceptor}$ and I_{donor} are fluorescence intensities around the emission maxima of the acceptor (660 nm) and donor fluorophore (600 nm), respectively. Measurements were performed at 20 ºC with ~200 nM labelled protein dissolved in buffer A.

Protein labelling for FRET measurements. Stochastic labelling was performed with the maleimide derivative of dyes Cy3B (GE Healthcare) and ATTO647N (ATTO-TEC) for OpuAC. The proteins MalE, SBD1, SBD2, OppA and PsaA were labelled with Alexa555 and Alexa647 maleimide (ThermoFisher). The purified proteins were first treated with 10 mM DTT for 30 min to fully reduce oxidized cysteines. After dilution of the protein sample to a DTT concentration of 1 mM the reduced protein was immobilized on a Ni^{2+}-Sepharose resin and washed with ten column volumes of buffer A (50 mM Tris-HCl, pH 7.4, 50 mM KCl for MalE and OppA. 25 mM Tris-HCl, pH 8.0, 150 mM NaCl, 1 µM EDTA for PsaA. 50 mM KPi, pH 7.4, 50 mM KCl for OpuAC, SBD1 and SBD2) to remove the DTT. To make sure that no endogenous substrate was left, for some experiments, and prior to removing the DTT, we unfolded the immobilized-SBPs by treatment with 6 M urea supplemented with 1 mM DTT and refolded them again by washing with buffer A. The resin was incubated 1-8 h at 4 °C with the dyes dissolved in buffer A. To ensure a high labelling efficiency, the dye concentration was ~20-times higher than the protein concentration. Subsequently, unbound dyes were removed by washing the column with at least twenty column volumes of buffer A. Elution of the proteins was done by supplementing buffer A with 400 mM imidazole. The labelled proteins were further purified by size-exclusion chromatography (Superdex 200, GE Healthcare) using buffer A. Sample composition was assessed by recording the absorbance at 280 nm (protein), 559 nm (donor), and 645 nm (acceptor) to estimate the labelling efficiency. For all proteins the labelling efficiency was ~90%. Anisotropies were determined as described in ref. 29 and were equal to or less than 0.23 for all fluorophores and proteins.

Solution-based smFRET and ALEX. Solution-based smFRET and alternating laser excitation (ALEX)[49] experiments were carried out at 25-100 pM of labelled protein at room temperature in buffer A supplemented with additional reagents as stated in the text. Microscope cover slides (no. 1.5H precision cover slides, VWR Marienfeld) were coated

with 1 mg/mL BSA for 30-60 s to prevent fluorophore and/or protein interactions with the glass material. Excess BSA was subsequently removed by washing and exchange with buffer A. All smFRET experiments were performed using a home-built confocal microscope. In brief, two laser-diodes (Coherent Obis) with emission wavelength of 532 and 637 nm were directly modulated for alternating periods of 50 µs and used for confocal excitation. The laser beams were coupled into a single-mode fibre (PM-S405-XP, Thorlabs) and collimated (MB06, Q-Optics/Linos) before entering a water immersion objective (60X, NA 1.2, UPlanSAPO 60XO, Olympus). The fluorescence was collected by excitation at a depth of 20 µm. Average laser powers were 30 µW at 532 nm (~30 kW/cm^2) and 15 µW at 637 nm (~15 kW/cm^2). Excitation and emission light was separated by a dichroic beam splitter (zt532/642rpc, AHF Analysentechnik), which is mounted in an inverse microscope body (IX71, Olympus). Emitted light was focused onto a 50 µm pinhole and spectrally separated (640DCXR, AHF Analysentechnik) onto two single-photon avalanche diodes (TAU-SPADs-100, Picoquant) with appropriate spectral filtering (donor channel: HC582/75; acceptor channel: Edge Basic 647LP; AHF Analysentechnik). Registration of photon arrival times and alternation of the lasers was controlled by an NI-Card (PXI-6602, National Instruments).

An individual labelled protein diffusing through the confocal volume generates a burst of photons. To identify fluorescence bursts a 'dual-channel burst search'[70] was used with parameters M = 15, T = 500 µs and L = 25. In brief, a fluorescent signal is considered a burst, when a total of L photons having M neighbouring photons within a time window of length T centred on their own arrival time. A first burst search was done that includes the donor and acceptor photons detected during the donor excitation, and a second burst search was done including only the acceptor photons detected during the acceptor excitation. The two separate burst searches were combined to define intervals when both donor and acceptor fluorophores are active. These intervals define the bursts. Only bursts having >150 photons were further analysed.

Three photon counts per burst were measured: N'_{DA} (acceptor emission upon donor excitation), N'_{DD} (donor emission upon donor excitation) and N'_{AA} (acceptor emission upon acceptor excitation) and assignment is based on the excitation period and detection channel[49]. The apparent FRET efficiency is calculated via $N'_{DA} / (N'_{DD} + N'_{DA})$ and the Stoichiometry S by $(N'_{DA} + N'_{DD}) / (N'_{DD} + N'_{DA} + N'_{AA})$[49]. The accurate FRET efficiency E was calculated by correcting the apparent FRET efficiency for background, direct excitation of the acceptor, leakage of donor fluorescence in the acceptor detection channel and relative differences in the efficiencies of the detectors and the quantum yield of the dyes[71]. Corrections were made using established protocols as described in Lee et al[71]. From the average E (see below) the

mean interprobe distance R was calculated via $E = 1/(1+(R/R_0)^6)$, using R_0 of 5.1 nm for Alexa555/Alexa647 and 6.2 nm for Cy3B/ATTO647N.

Binning the detected bursts into a 2D (apparent) FRET/S histogram allowed the selection of the donor and acceptor labelled molecules and reduce artefacts arising from fluorophore bleaching[49]. The selected (apparent) FRET histogram were fitted with a Gaussian distribution using nonlinear least square, to obtain a 95% confidence interval for the distribution mean.

Scanning confocal microscopy. Excitation was achieved with a spectrally filtered laser beam of a pulsed supercontinuum source (SuperK Extreme, NKT Photonics) with an acousto-optical tuneable filter (AOTFnc-VIS, EQ Photonics), which led to excitation pulses centred at 532 nm. The beam was coupled into a single-mode fibre (PM-S405-XP, Thorlabs) and the collimated beam (Focussing collimator MB06, Q-Optics/Linos) was coupled into an oil-immersion objective (60×, NA 1.35, UPLSAPO 60XO, Olympus) by using a dichroic beam splitter (zt532/642rpc, AHF Analysentechnik) mounted on an inverse microscope body (IX71, Olympus). Data were recorded with constant 532 nm excitation at an intensity of 0.5 µW (~125 W/cm^2) for SBD1, SBD2, PsaA, OppA and MalE, but 1.5 µW (~400 W/cm^2) for OpuAC. Surface scanning was performed by using a XYZ-piezo stage with 100×100×20 µm range (P-517-3CD with E-725.3CDA, Physik Instrumente). Emitted light was focused onto a 50 µm pinhole and spectrally separated (640DCXR, AHF Analysentechnik) onto two single-photon avalanche diodes (TAU-SPADs-100, Picoquant) with appropriate spectral filtering (donor channel: HC582/75 and acceptor channel: ET700/75; AHF Analysentechnik). The detector signal was registered by using a HydraHarp 400 multichannel picosecond event timer and a module for time-correlated single photon counting (both Picoquant). Scanning images of 10×10 µm were recorded with 50 nm step size and 2 ms integration time at each pixel. After each surface scan, the positions of labelled proteins were identified manually; the position information was used to subsequently generate fluorescence trajectories.

Microscope cover-slides (No. 1.5, Marienfeld, Germany) were cleaned by sonication in subsequently ethanol, acetone and MQ water for 10 min each, followed by plasma etching (Plasma Etch, PE-25- JW) for 10 min. Functionalization with PEG-Silane (6-9 PE units) and Biotin-PEG-Silane (MW3400, Laysan Inc.) was done in toluene (55 °C; o/n) and flow cells were assembled according to ref[29, 72]. To immobilize the labelled proteins within these flow cells, the surfaces were first incubated for 10 min with a solution containing 0.2 mg/ml neutravidin (Invitrogen) in buffer A. Unbound neutravidin was washed away with buffer A. Next, the surface was incubated with 1 nM biotinylated penta-His antibody (Qiagen) in buffer A for 10 min. Then, labelled proteins were immobilized by incubating with 5-50 pM of labelled protein in buffer A for 5 min. Unbound proteins were washed away with buffer A.

MalE was studied on standard functionalized cover-slides, since MalE was extremely sensitive to contaminations of maltodextrins in double-sided tape or other flow-cell parts. All experiments of OpuAC and PsaA were carried out in degassed buffer A supplemented with 10 mM of (±)-6-Hydroxy-2,5,7,8-tetramethylchromane-2-carboxylic acid (Trolox) and under oxygen-free conditions, obtained via an oxygen-scavenging system. For the other SBPs, experiments were performed in buffer A with 1 mM Trolox and 10 mM Cysteamine.

Analysis of fluorescence trajectories. The fluorescence trajectories were analysed by integrating the detected red and green photon streams in time-bins as stated throughout the text and/or figure captions. Only traces lasting longer than 50 time-bins, having on average more than 10 photons per time-bin and showed clear bleaching steps, were used for further analysis. The number of analysed molecules, transitions and the total observation time are indicated in Table S2.3. The apparent FRET per time-bin was calculated by dividing the red photons by the total number of photons per time-bin. The state-trajectory of the FRET time-trace was modelled by a Hidden Markov Model (HMM)[73]. For this an implementation of HMM was programmed in MATLAB (MathWorks), based on the work of Rabiner[73]. In the analysis, we assumed that the FRET time-trace (the observation sequence) can be considered as an HMM with two states having a one-dimensional Gaussian-output distribution. The Gaussian output-distribution of state i (i =1, 2) is parameterized by the mean and variance. The maximum likelihood estimates of the parameters λ (transition probabilities that connect the states and parameters of output-distribution) was iteratively found using the Baum-Welch algorithm, which is an implementation of the Expectation-Maximisation algorithm[74]. Care was taken to avoid floating point underflow and was done as described[73]. With the maximum likelihood estimate of λ, the most probable state-trajectory is then found using the Viterbi algorithm[75]. The time spent in each state (open, closed) was inferred from the most probable state-trajectory.

2.5 Author contribution

M.d.B., G.G., B.P., C.A.M. and T.C. designed the project. B.P., C.A.M. and T.C. supervised the project. M.d.B., G.G., R.V. and F.H. performed the molecular biology and protein chemistry studies and developed the labelling protocols. M.d.B., G.G., R.V., F.H. and N.E. performed single-molecule experiments. M.d.B. analysed the single-molecule data. G.K.S. performed transport assays and ITC. S.L.B. and C.A.M. designed and executed the PsaA biochemical studies. All authors contributed to discussion of the results and writing of the manuscript.

2.6 Supplementary Information

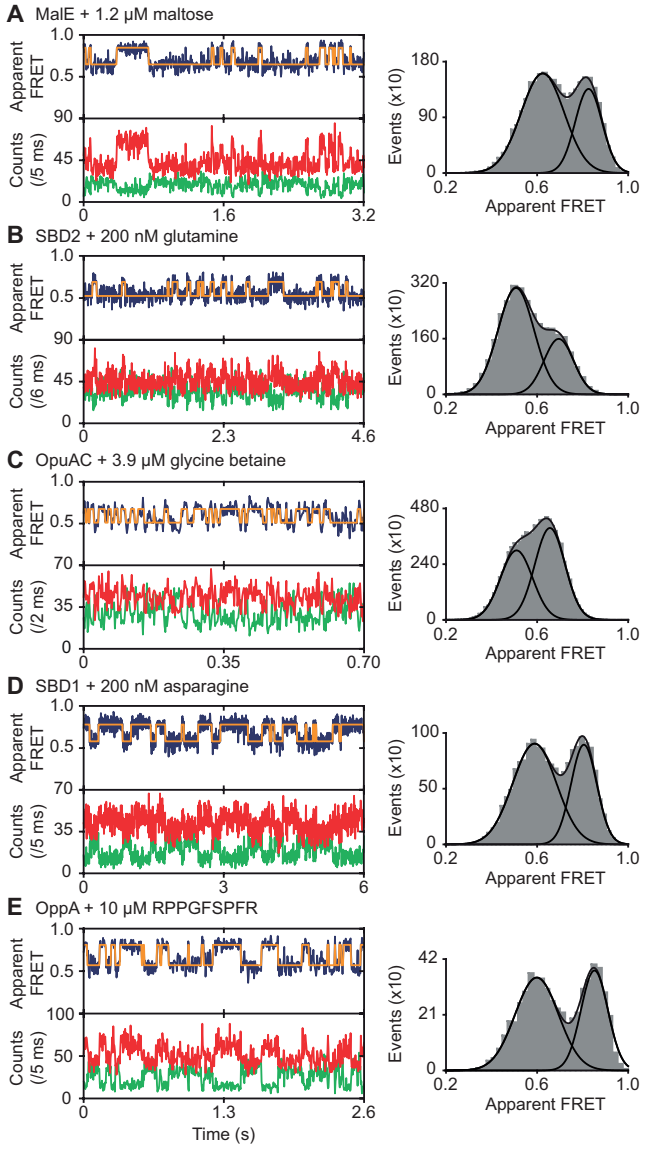

Figure S2.1. Substrate-induced conformational dynamics of SBPs. (A-E) Fluorescence trajectories (left) and apparent FRET efficiency histograms from all fluorescence trajectories (right) of the indicated SBPs and indicated substrate concentrations. In the fluorescence trajectories: the top panel shows the calculated apparent FRET efficiency (blue) from the donor (green) and acceptor (red) photon counts as shown in the bottom panels. The most probable state-trajectory of the HMM is shown by the orange line. Statistics can be found in Table S2.3. The histogram was fitted with two Gaussian distributions to obtain the relative population of the high FRET state. We ignored the small contribution of intrinsic closing (Figure 2.3H) and used the one site-binding model to determine K_D (Table S2.1).

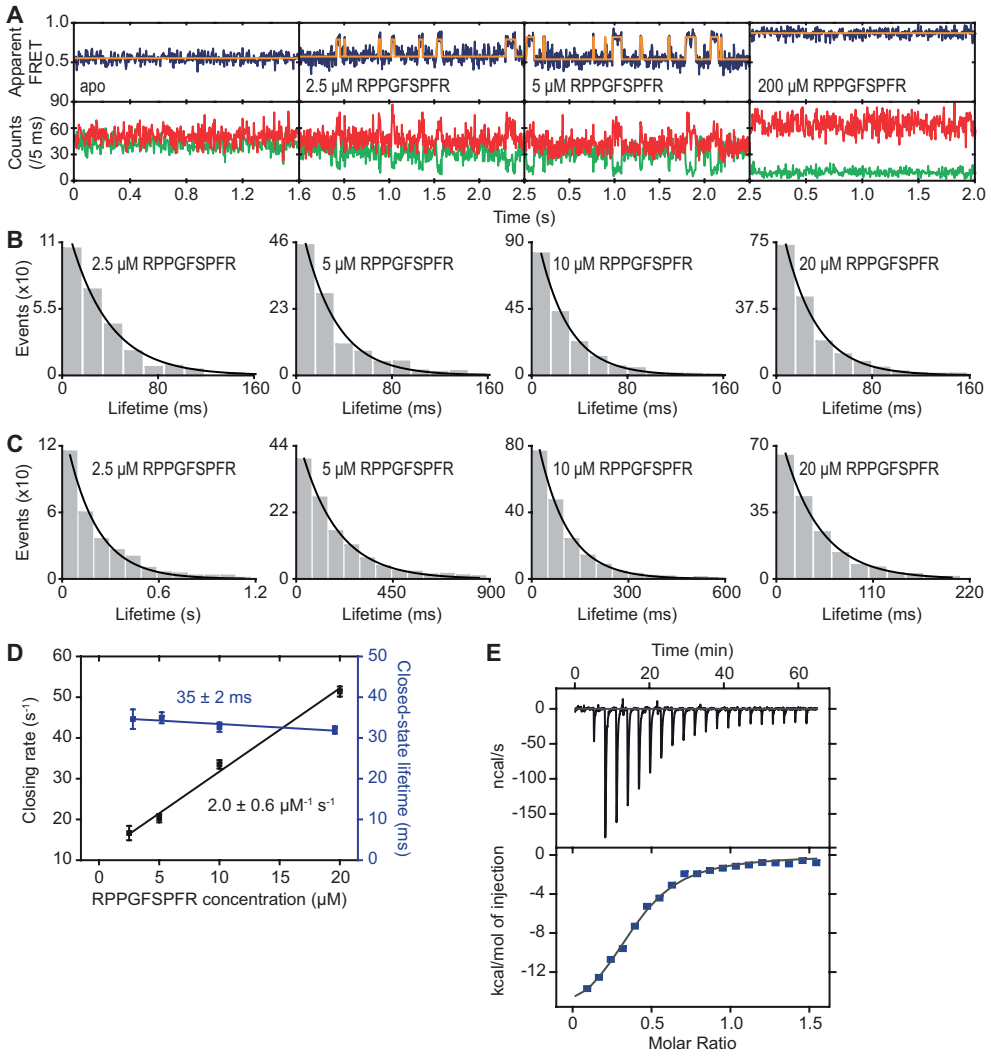

Figure S2.2. OppA uses the induced-fit mechanism. (A) Representative fluorescence trajectories of OppA(A209C/S441C) at different peptide (RPPGFSFR) concentrations; donor (green) and acceptor (red) photon counts. The top panel shows the calculated apparent FRET efficiency (blue) with the most probable state-trajectory of the HMM (orange). Lifetime histogram of the high FRET state (closed conformation) (B) and low FRET state (open conformation) (C) as obtained from the most probable state-trajectory of the HMM. Bars are the data and the solid line is an exponential fit. Statistics can be found in Table S2.3. (D) Average closing rate (rate from low to high FRET state; black) and average lifetime of the substrate-bound conformation (lifetime high FRET state; purple). Data correspond to mean ± s.e.m. and the solid line is a linear fit. Slope and intercept of the fit are shown (95% confidence interval). From the fit a K_D of 14 ± 5 µM (95% confidence interval) is obtained. (E) Isothermal calorimetry binding isotherm of the titration of OppA with RPPGFSFR, obtaining K_D of 5 ± 3 µM (mean ± s.d., n = 3). Points are the data and the solid line is a fit to a one site-binding model.

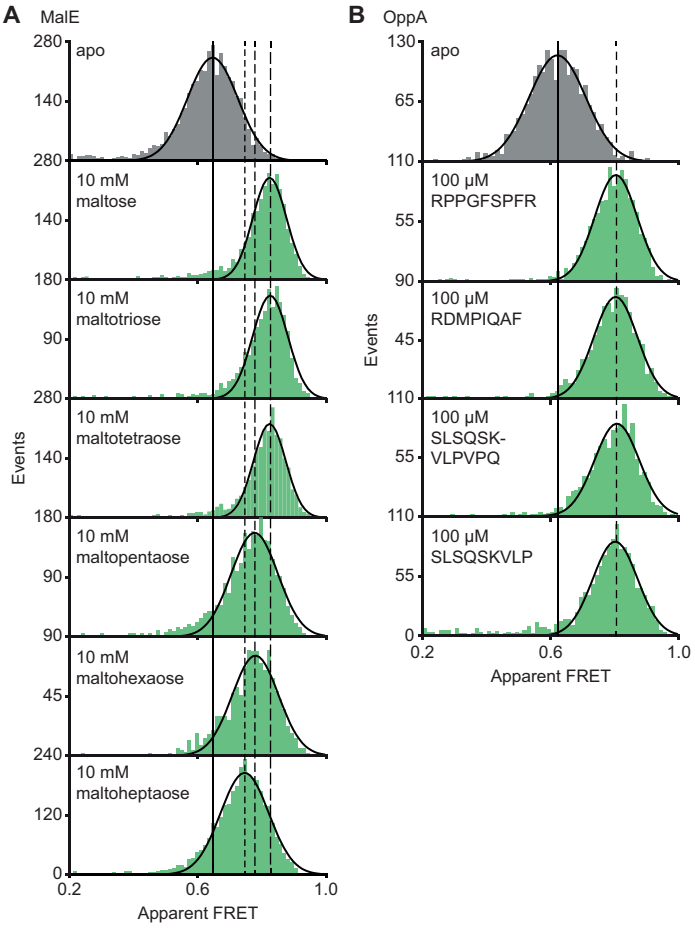

Figure S2.3. Translocation competent conformation(s) of MalE and OppA. Solution-based apparent FRET efficiency histogram of MalE(T36C/S352C) (A) and OppA(A209C/S441C) (B) in the absence and presence of different cognate substrates as indicated. The OppA substrates are indicated by one-letter amino acid code. Bars are the data and solid line a Gaussian fit. The 95% confidence interval for the mean of the Gaussian distribution is shown in Table S2.2, and the interval centers are indicated by vertical lines (solid and dashed).

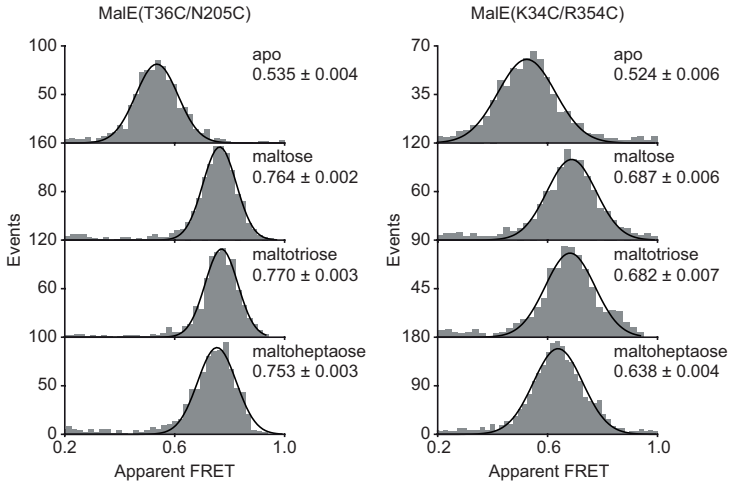

Figure S2.4. MalE conformations studied by smFRET. Solution-based apparent FRET efficiency histogram of MalE(T36C/N205C) (left) and MalE(K34C/R354C) (right) in the absence and presence of different cognate substrates as indicated. Bars are the data and the solid line a Gaussian fit. A 95% confidence interval for the mean is indicated

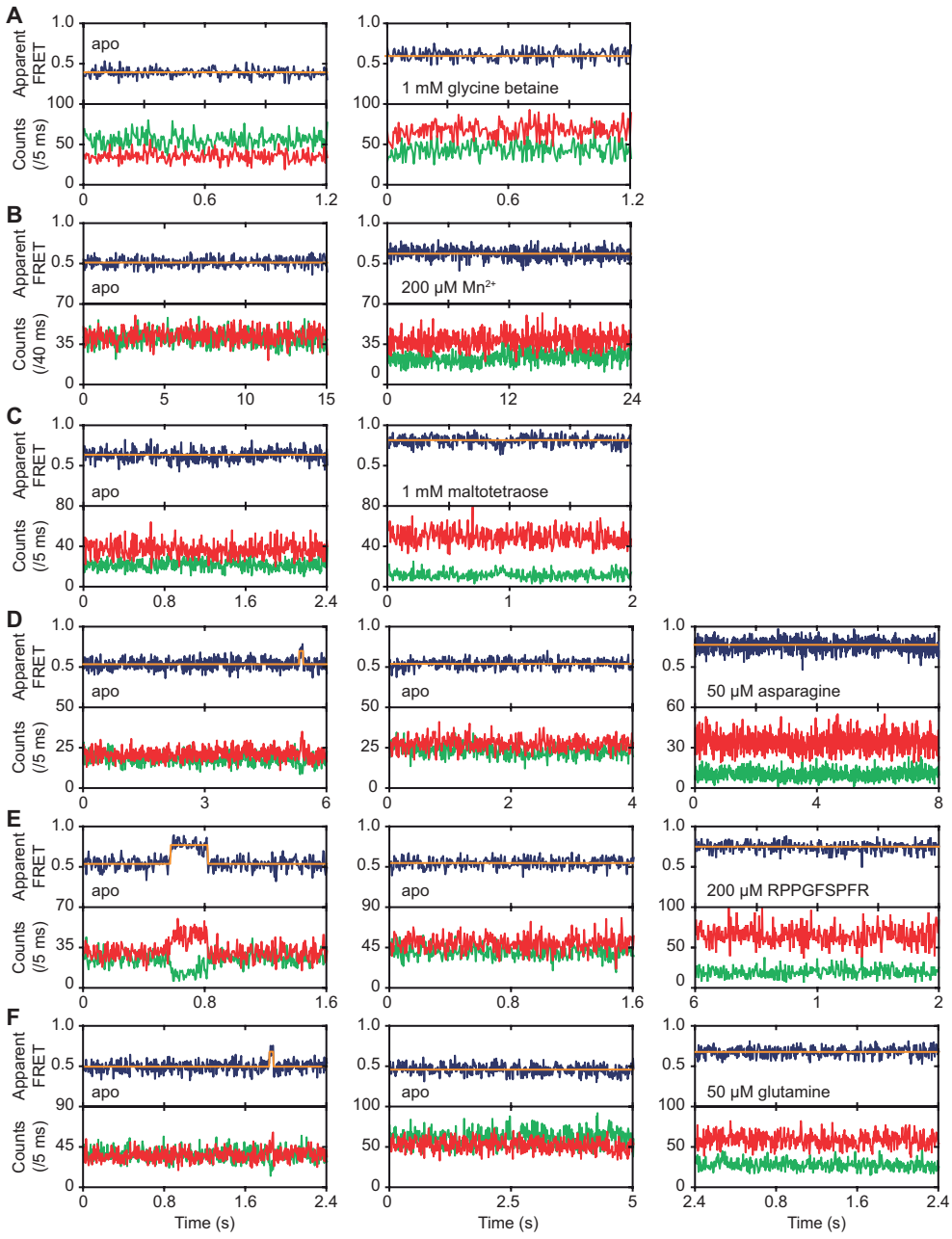

Figure S2.5. Conformational dynamics of substrate-free and substrate-bound SBPs. Fluorescence trajectories of OpuAC(V360C/N423C) (A), PsaA(V76C/K237C) (B), MalE(T36C/S352C) (C), SBD1(T159C/G87C) (D), OppA(A209C/S441C) (E) and SBD2(T369C/S451) (F). In the absence of substrate, 10-20 μM of unlabelled protein or 1 mM EDTA (for PsaA) was added. The top panels show the calculated apparent FRET efficiency (blue) from the donor (green) and acceptor (red) photon counts as presented in bottom panels. The orange line indicates the average apparent FRET efficiency value or the most probable state-trajectory of the HMM. Statistics can be found in Table S2.3.

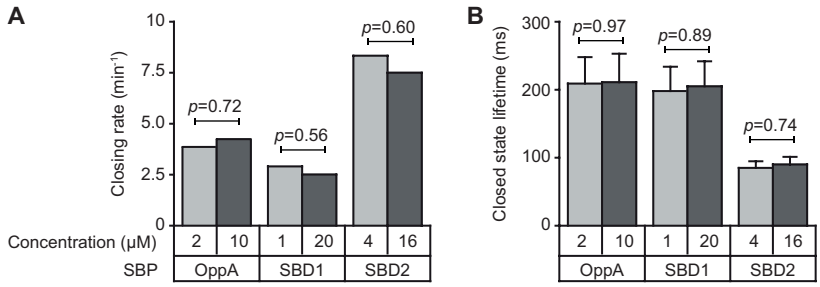

Figure S2.6. Intrinsic conformational dynamics in the presence of unlabelled protein. Closing rate (A) and average lifetime of the closed conformation (B) in the absence of substrate and in the presence of different concentrations of unlabelled protein to scavenge potential substrate contaminations. Examples of the high FRET transitions are shown in Figure 2.3 and Figure S2.5. Error bars correspond to s.e.m.. The closing rate was determined by dividing the total number of high FRET transitions by the total observation time of all molecules. The statistical significance of the closing rate was determined by testing for the difference in the proportion of time-bins in which a low to high FRET transition is made and using the *z*-test. The statistical significance of the average closed state lifetime was determined by a two-tailed unpaired *t*-tests.

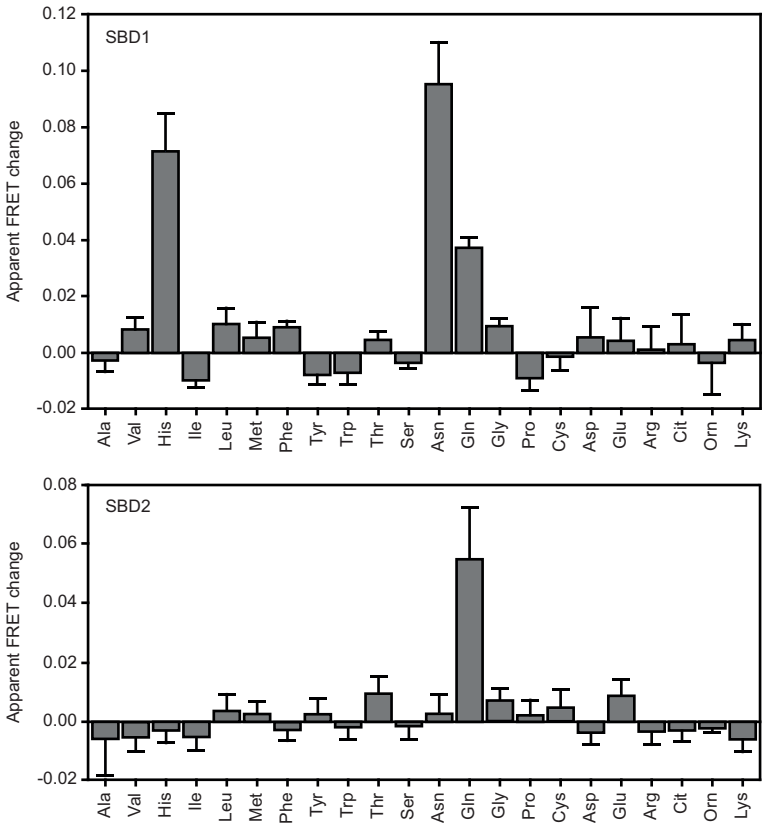

Figure S2.7. Substrate binding studied by ensemble FRET. The mean apparent FRET changes of SBD1 (top) and SBD2 (bottom) in the presence of 5 mM of the indicated amino acids relative to their absence. Amino acids are indicated by their three letter abbreviation. Data correspond to mean ± s.d. of the apparent FRET change of duplicate measurements with the same labelled protein sample.

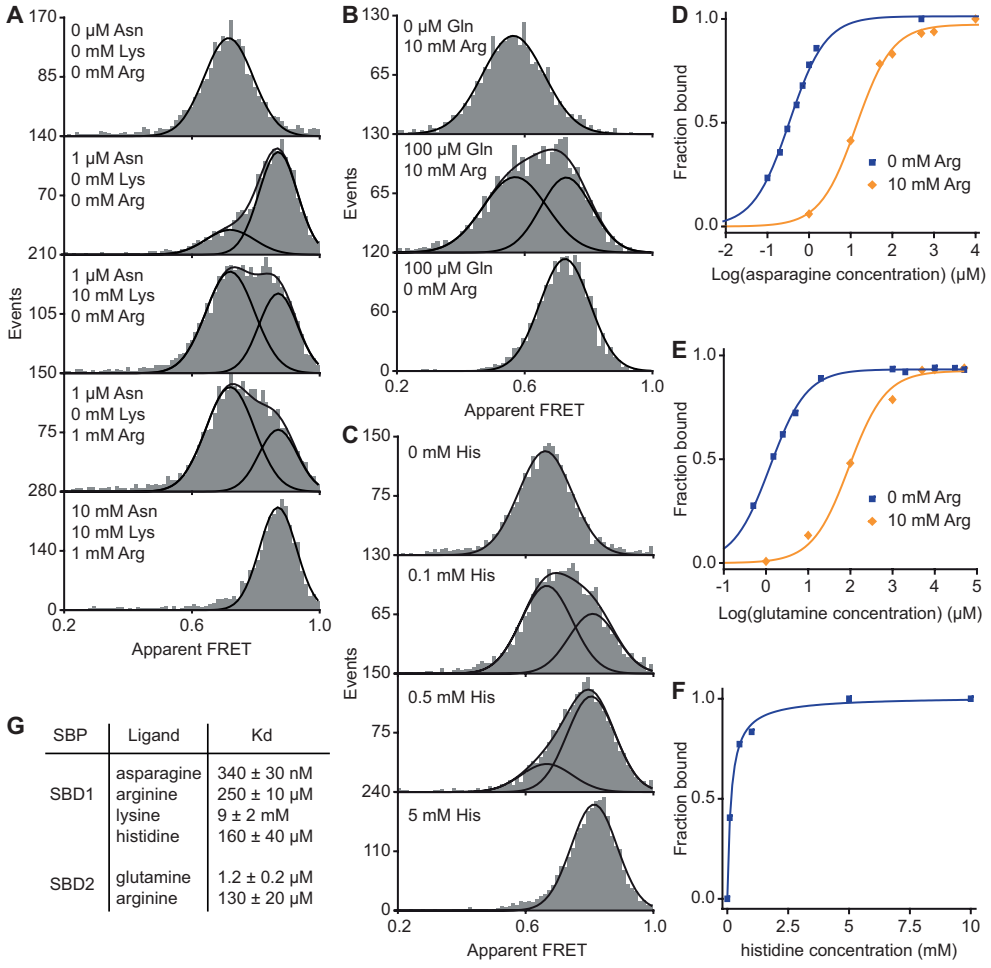

G

SBP	Ligand	Kd
SBD1	asparagine	340 ± 30 nM
	arginine	250 ± 10 µM
	lysine	9 ± 2 mM
	histidine	160 ± 40 µM
SBD2	glutamine	1.2 ± 0.2 µM
	arginine	130 ± 20 µM

Figure S2.8. Non-cognate substrate binding by SBD1 and SBD2. Solution-based apparent FRET efficiency histograms of SBD1(T159C/G87C) (A and C) and SBD2(T369C/S451) (B) in the presence of different substrate concentrations as indicated. Bars are the data and the solid lines a fit to a mixture model with two Gaussian distributions or a fit with a single Gaussian distribution as shown. The mean of the Gaussian distributions was obtained from the extreme conditions and fixed in the mixture model. Fraction of SBD1 bound to asparagine (D), SBD2 bound to glutamine (E) and SBD1 bound to histidine (F). Points are the data and the solid line a fit to a one site-binding model. (G) Estimated dissociation constants K_D as obtained from the fit. Error bars represent a 95% confidence interval.

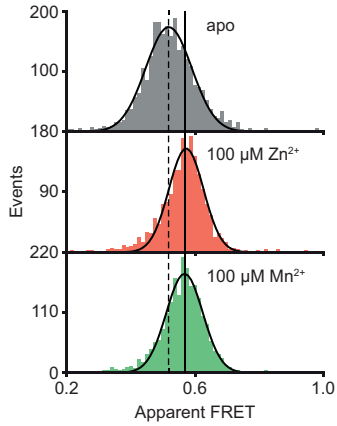

Figure S2.9. PsaA(E74C/K237C) conformational changes probed by smFRET. Solution-based apparent FRET efficiency histogram of PsaA(E74C/K237C) in the presence and absence of metal ions as indicated. Bars are the data and solid line a Gaussian fit. The 95% confidence interval for the distribution mean is shown in Table S2.2. The interval center is indicated by a vertical line (solid and dashed).

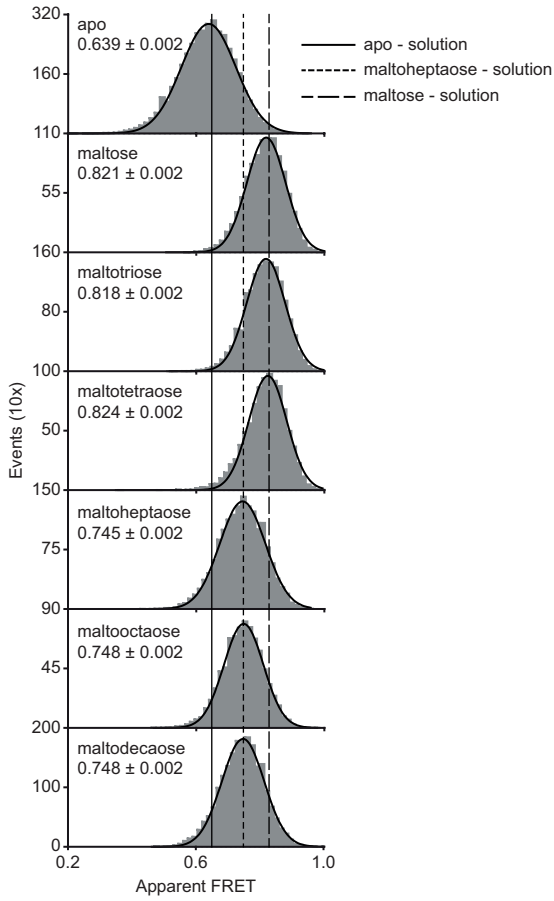

Figure S2.10. Surface-based smFRET histogram of MalE. Surface-based apparent FRET efficiency histogram of MalE(T36C/S352C) in the presence of different maltodextrin substrates as indicated. From the most probable state-trajectory of the HMM the apparent FRET efficiencies of the low (substrate-free conformation) and high FRET state (closed substrate-bound conformation) were obtained and used for the histogram. The histogram was constructed from all fluorescence trajectories. Representative fluorescence trajectories are shown in Figure 2.6B-G. Bars are the data and solid line a Gaussian fit. The 95% confidence interval for the distribution mean is indicated. The average apparent FRET efficiencies of the solution-based smFRET measurements (Figure S2.3A) are indicated by vertical lines.

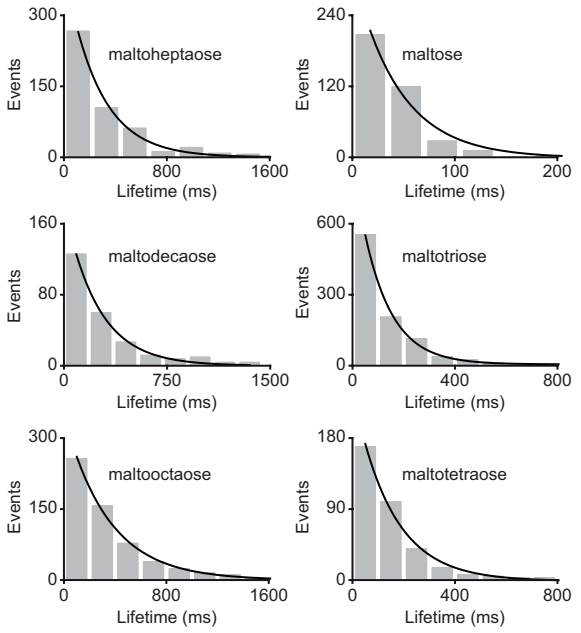

Figure S2.11. Distribution of the substrate-bound conformations of MalE. Lifetime histogram of the high FRET state as obtained from the most probable state-trajectory of the HMM of all molecules per condition as shown in Figure 2.6B-G. Grey bars are the data and the solid line an exponential fit. Statistics can be found in Table S2.3.

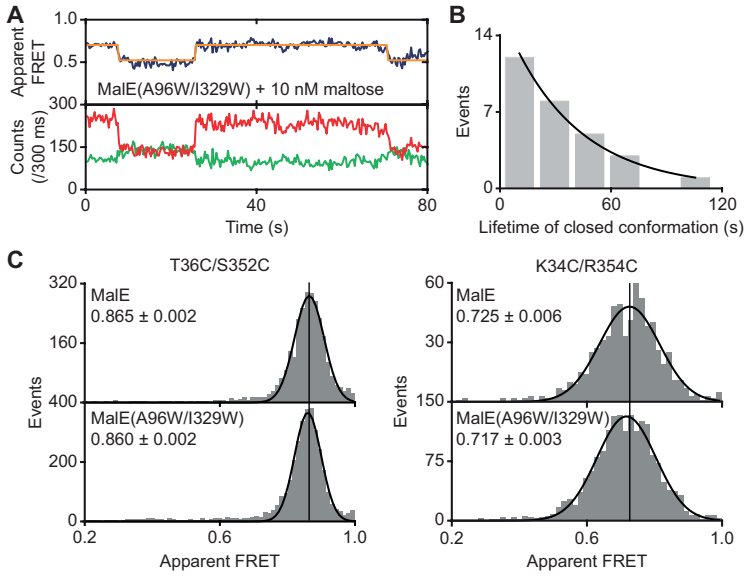

Figure S2.12. Conformational changes of MalE(A96W/I329W). (A) Fluorescence trajectory of MalE(T36C/S352C/A96W/I329W). The top panel shows the apparent FRET efficiency (blue) and the donor (green) and acceptor (red) photon counts are shown in the bottom panel. The most probable state-trajectory of the HMM is shown (orange). (B) Lifetime histogram of the high FRET state. Solid line is an exponential fit. (C) Solution-based apparent FRET efficiency histogram of MalE and MalE(A96W/I329W) in the presence of 1 mM maltose for the indicated interprobe positions. Bars are the data and solid line a Gaussian fit. The 95% confidence interval for the mean of the Gaussian distribution is indicated. The FRET distributions of the wild type and mutant proteins are not significantly different; p=0.28 (T36C/S352C) and p=0.30 (K34C/R354C) using the two-way KS test.

Table S2.1. Dissociation constant K_D of SBPs

		K_D (μM)		
Protein[a]	Substrate	Freely-diffusing	Surface-tethered	K_D WT[f] (μM)
OpuAC(V360C/N423C)	glycine betaine	3.4 ± 0.4[b]	3.1[c]	4-5[38]
OppA(A209C/S441C)	RPPGFSFR	7.0 ± 1[b]	14 ± 5[e]	5 ± 3[e]
SBD2(T369C/S451)	glutamine	1.2 ± 0.2[d]	0.5[c]	0.9 ± 0.1[29]
SBD1(T159C/G87C)	asparagine	0.34 ± 0.03[d]	0.3[c]	0.2 ± 0.0[29]
MalE(T36C/S352C)	maltose	1.7 ± 0.3[b]	2.2[c]	1-2[16, 32]
MalE(T36C/S352C)	maltotriose	0.6 ± 0.2[b]	0.9[c]	0.2-2[16, 32]

a. K_D could not be determined reliably for labelled PsaA due to metal contaminations.
b. Population of the closed conformation P in the presence of a substrate concentration L was determined using solution-based smFRET. The $K_D = L\,(1-P)/P$ for a one-binding site model. Data corresponds to mean ± s.d. of duplicate experiments with the same protein sample.
c. Figure S2.1
d. Figure S2.8
e. Figure S2.2
f. The K_D values of wild type (WT) proteins are obtained from the indicated references.

Table S2.2. Apparent FRET efficiency values of solution-based measurements

Protein[a]	Condition	Apparent FRET[b]	Interprobe distance change (Å)[b]	Cα-Cα distance change in crystal (Å)[c]
OpuAC(V360C/N423C)	no substrate	0.501 ± 0.004		
	carnitine	0.479 ± 0.003	-1.2 ± 0.3	
	proline	0.543 ± 0.004	3.4 ± 0.3	
	glycine betaine	0.646 ± 0.003	9.0 ± 0.3	9.4
SBD2(T369C/S451)	no substrate	0.492 ± 0.003		
	glutamate	0.633 ± 0.004	7.2 ± 0.4	9.3
	glutamine	0.677 ± 0.002	9.4 ± 0.4	
	arginine	0.496 ± 0.002	0.0 ± 0.3	
SBD1(G87C/T159C)	no substrate	0.612 ± 0.003		
	glutamine	0.710 ± 0.003	4.6 ± 0.6	
	asparagine	0.805 ± 0.002	9.4 ± 1.2	
	histidine	0.761 ± 0.003	7.2 ± 1.0	
	arginine	0.610 ± 0.002	0.0 ± 0.4	
	lysine	0.613 ± 0.002	0.0 ± 0.4	
MalE(T36C/S352C)	no substrate	0.646 ± 0.003		
	β-cyclodextrin	0.696 ± 0.003	2.7 ± 0.2	
	maltotriitol	0.725 ± 0.003	3.7 ± 0.2	
	maltotetraitol	0.725 ± 0.003	3.7 ± 0.2	
	maltose	0.824 ± 0.002	9.8 ± 0.3	10.2
	maltotriose	0.826 ± 0.003	9.7 ± 0.3	
	maltotetraose	0.824 ± 0.002	9.6 ± 0.3	
	maltopentaose	0.777 ± 0.004	6.8 ± 0.3	
	maltohexaose	0.779 ± 0.003	6.8 ± 0.2	
	maltoheptaose	0.746 ± 0.002	5.2 ± 0.2	
	maltooctaose	0.745 ± 0.003	5.1 ± 0.2	
	maltodecaose	0.742 ± 0.003	5.2 ± 0.2	
MalE(T36C/N205C)	no substrate	0.538 ± 0.007		
	maltoheptaose	0.755 ± 0.005	6.4 ± 0.5	
	maltooctaose	0.758 ± 0.005	6.5 ± 0.5	
	maltodecaose	0.757 ± 0.006	6.4 ± 0.5	
MalE(K34C/R354C)	no substrate	0.524 ± 0.010		
	maltoheptaose	0.669 ± 0.008	8.7 ± 0.6	
	maltooctaose	0.662 ± 0.007	8.8 ± 0.6	
	maltodecaose	0.666 ± 0.008	8.8 ± 0.6	
OppA(A209C/S441C)	no substrate	0.621 ± 0.004		
	RPPGFSPFR	0.803 ± 0.003	9.3 ± 0.4	12.7
	RDMPIQAF	0.803 ± 0.003	9.2 ± 0.4	
	SLSQSKVLPVPQ	0.807 ± 0.004	9.3 ± 0.4	
	SLSQSKVLP	0.801 ± 0.003	9.3 ± 0.4	
PsaA(V76C/K237C)	no substrate	0.615 ± 0.003		
	Mn^{2+}	0.681 ± 0.004	4.0 ± 0.4	3.8
	Zn^{2+}	0.688 ± 0.004	4.1 ± 0.4	
PsaA(E74C/K237C)	no substrate	0.518 ± 0.003		
	Mn^{2+}	0.567 ± 0.003	3.2 ± 0.3	3.5
	Zn^{2+}	0.570 ± 0.003	3.2 ± 0.3	
PsaA(D280N/V76C/K237)	no substrate	0.617 ± 0.003		
	Zn^{2+}	0.689 ± 0.005	4.1 ± 0.4	

a. Only data of the same construct can be compared, due to differences in microscope settings.
b. Error denotes 95% confidence interval for the mean.
c. Distance calculated from crystal structures with PDB codes: OpuAC (3L6G, 3L6H), SBD2 (4KR5, 4KQP), PsaA (3ZK7, 1PSZ), OppA (3FTO, 3DRG) and MalE (1OMP, 1ANF).

Table S2.3. Statistics of confocal scanning experiments of immobilized molecules

Protein[a]	Condition[b]	Molecules analysed	Total time (min)	Transitions observed
OpuAC(V360C/N423C)	no substrate + 20 µM protein	702	8.2	0
	3.9 µM glycine betaine	102	1.2	2692
	1 mM glycine betaine	94	2.3	0
OppA(A209C/S441C)	no substrate + 2 µM protein	202	6.4	21
	no substrate + 10 µM protein	311	6.6	26
	2.5 µM RPPGFSPFR	43	1.4	267
	5 µM RPPGFSPFR	168	4.6	1080
	10 µM RPPGFSPFR	143	4.5	1800
	20 µM RPPGFSPFR	76	2.2	1683
	200 µM RPPGFSPFR	31	0.5	0
SBD1(G87C/T159C)	no substrate + 1 µM protein	133	6.2	18
	no substrate + 20 µM protein	292	20.6	50
	200 nM asparagine	22	1.5	207
	50 µM asparagine	72	8.0	0
SBD2(T369C/S451)	no substrate + 4 µM protein	148	6.1	51
	no substrate + 16 µM protein	166	5.1	38
	200 nM glutamine	23	1.8	498
	50 µM glutamine	82	1.0	0
MalE(T36C/S352C)	no substrate + 20 µM protein	503	10.9	0
	1 mM maltotetraose	32	1.2	0
	1.2 µM maltose	37	1.6	378
	400 nM maltotriose	144	7.2	968
	450 nM maltotetraose	70	1.8	345
	2 µM maltoheptaose	61	4.9	591
	2 µM maltooctaose	50	2.2	491
	4 µM maltodecaose	75	4.9	257
MalE(T36C/S352C/ A96W/I329W)	10 nM maltose	20	20.4	30
PsaA(76C/K237C)	no substrate + 1 mM EDTA	254	26.3	0
	200 µM Mn^{2+}	35	5.8	0

a. Fluorescence trajectories of 2 independent labelled proteins samples were pooled.
b. Unlabelled protein was added to study apo protein (details in Section 2.2.2).

2.7 References

1. Higgins, C. F. ABC transporters: from microorganisms to man. Annu. Rev. Cell Biol. 8, 67-113 (1992).

2. Berntsson, R. P., Smits, S. H., Schmitt, L., Slotboom, D. J. & Poolman, B. A structural classification of substrate-binding proteins. FEBS Lett. 584, 2606-2617 (2010).

3. Scheepers, G. H., Lycklama A Nijeholt, J. A. & Poolman, B. An updated structural classification of substrate-binding proteins. FEBS Lett. 590, 4393-4401 (2016).

4. van der Heide, T. & Poolman, B. ABC transporters: one, two or four extracytoplasmic substrate-binding sites? EMBO Rep. 3, 938-943 (2002).

5. Locher, K. P. Mechanistic diversity in ATP-binding cassette (ABC) transporters. Nat. Struct. Mol. Biol. 23, 487-493 (2016).

6. Swier, L. J. Y. M., Slotboom, D. J. & Poolman, B. in ABC transporters - 40 years on (ed George, A. M.) 3-36 (Springer International Publishing, 2016).

7. Davidson, A. L., Dassa, E., Orelle, C. & Chen, J. Structure, function, and evolution of bacterial ATP-binding cassette systems. Microbiol. Mol. Biol. Rev. 72, 317-64 (2008).

8. Shilton, B. H., Flocco, M. M., Nilsson, M. & Mowbray, S. L. Conformational changes of three periplasmic receptors for bacterial chemotaxis and transport: the maltose-, glucose/galactose- and ribose-binding proteins. J. Mol. Biol. 264, 350-363 (1996).

9. Quiocho, F. A. & Ledvina, P. S. Atomic structure and specificity of bacterial periplasmic receptors for active transport and chemotaxis: variation of common themes. Mol. Microbiol. 20, 17-25 (1996).

10. Karpowich, N. K., Huang, H. H., Smith, P. C. & Hunt, J. F. Crystal structures of the BtuF periplasmic-binding protein for vitamin B12 suggest a functionally important reduction in protein mobility upon ligand binding. J. Biol. Chem. 278, 8429-8434 (2003).

11. Trakhanov, S. et al. Ligand-free and -bound structures of the binding protein (LivJ) of the Escherichia coli ABC leucine/isoleucine/valine transport system: trajectory and dynamics of the interdomain rotation and ligand specificity. Biochemistry 44, 6597-6608 (2005).

12. Nishitani, Y. et al. Recognition of heteropolysaccharide alginate by periplasmic solute-binding proteins of a bacterial ABC transporter. Biochemistry 51, 3622-3633 (2012).

13. Pandey, S., Modak, A., Phale, P. S. & Bhaumik, P. High resolution structures of periplasmic glucose-binding protein of Pseudomonas putida CSV86 reveal structural basis of its substrate specificity. J. Biol. Chem. 291, 7844-7857 (2016).

14. Magnusson, U., Salopek-Sondi, B., Luck, L. A. & Mowbray, S. L. X-ray structures of the leucine-binding protein illustrate conformational changes and the basis of ligand specificity. J. Biol. Chem. 279, 8747-8752 (2004).

15. Quiocho, F. A., Spurlino, J. C. & Rodseth, L. E. Extensive features of tight oligosaccharide binding revealed in high-resolution structures of the maltodextrin transport/chemosensory receptor. Structure 5, 997-1015 (1997).

16. Hall, J. A., Ganesan, A. K., Chen, J. & Nikaido, H. Two modes of ligand binding in maltose-binding protein of Escherichia coli. Functional significance in active transport. J. Biol. Chem. 272, 17615-17622 (1997).

17. Hall, J. A., Thorgeirsson, T. E., Liu, J., Shin, Y. K. & Nikaido, H. Two modes of ligand binding in maltose-binding protein of Escherichia coli. Electron paramagnetic resonance study of ligand-induced global conformational changes by site-directed spin labeling. J. Biol. Chem. 272, 17610-17614 (1997).

18. Sharff, A. J., Rodseth, L. E. & Quiocho, F. A. Refined 1.8-A structure reveals the mode of binding of beta-cyclodextrin to the maltodextrin binding protein. Biochemistry 32, 10553-10559 (1993).

19. Skrynnikov, N. R. et al. Orienting domains in proteins using dipolar couplings measured by liquid-state NMR: differences in solution and crystal forms of maltodextrin binding protein loaded with beta-cyclodextrin. J. Mol. Biol. 295, 1265-1273 (2000).

20. Oldham, M. L., Chen, S. & Chen, J. Structural basis for substrate specificity in the Escherichia coli maltose transport system. Proc. Natl. Acad. Sci. U. S. A. 110, 18132-18137 (2013).

21. Yu, J., Ge, J., Heuveling, J., Schneider, E. & Yang, M. Structural basis for substrate specificity of an amino acid ABC transporter. Proc. Natl. Acad. Sci. U. S. A. 112, 5243-5248 (2015).

22. Woo, J. S., Zeltina, A., Goetz, B. A. & Locher, K. P. X-ray structure of the Yersinia pestis heme transporter HmuUV. Nat. Struct. Mol. Biol. 19, 1310-1315 (2012).

23. Pinkett, H. W., Lee, A. T., Lum, P., Locher, K. P. & Rees, D. C. An inward-facing conformation of a putative metal-chelate-type ABC transporter. Science 315, 373-377 (2007).

24. Locher, K. P., Lee, A. T. & Rees, D. C. The E. coli BtuCD structure: a framework for ABC transporter architecture and mechanism. Science 296, 1091-1098 (2002).

25. Flocco, M. M. & Mowbray, S. L. The 1.9 A x-ray structure of a closed unliganded form of the periplasmic glucose/galactose receptor from Salmonella typhimurium. J. Biol. Chem. 269, 8931-8936 (1994).

26. Oswald, C. et al. Crystal structures of the choline/acetylcholine substrate-binding protein ChoX from Sinorhizobium meliloti in the liganded and unliganded-closed states. J. Biol. Chem. 283, 32848-32859 (2008).

27. Tang, C., Schwieters, C. D. & Clore, G. M. Open-to-closed transition in apo maltose-binding protein observed by paramagnetic NMR. Nature 449, 1078-1082 (2007).

28. Feng, Y. et al. Conformational dynamics of apo-GlnBP revealed by experimental and computational analysis. Angew. Chem. Int. Ed Engl. 55, 13990-13994 (2016).

29. Gouridis, G. et al. Conformational dynamics in substrate-binding domains influences transport in the ABC importer GlnPQ. Nat. Struct. Mol. Biol. 22, 57-64 (2015).

30. Duan, X. & Quiocho, F. A. Structural evidence for a dominant role of nonpolar interactions in the binding of a transport/chemosensory receptor to its highly polar ligands. Biochemistry 41, 706-712 (2002).

31. Sooriyaarachchi, S., Ubhayasekera, W., Park, C. & Mowbray, S. L. Conformational changes and ligand recognition of Escherichia coli D-xylose binding protein revealed. J. Mol. Biol. 402, 657-668 (2010).

32. Kim, E. et al. A single-molecule dissection of ligand binding to a protein with intrinsic dynamics. Nat. Chem. Biol. 9, 313-318 (2013).

33. Seo, M. H., Park, J., Kim, E., Hohng, S. & Kim, H. S. Protein conformational dynamics dictate the binding affinity for a ligand. Nat. Commun. 5, 3724- (2014).

34. Husada, F. et al. Watching conformational dynamics of ABC transporters with single-molecule tools. Biochem. Soc. Trans. 43, 1041-1047 (2015).

35. Lerner, E. et al. Toward dynamic structural biology: two decades of single-molecule Forster resonance energy transfer. Science 359, aan1133 (2018).

36. Ha, T. et al. Probing the interaction between two single molecules: fluorescence resonance energy transfer between a single donor and a single acceptor. Proc. Natl. Acad. Sci. U. S. A. 93, 6264-6268 (1996).

37. Fulyani, F., Schuurman-Wolters, G. K., Slotboom, D. J. & Poolman, B. Relative rates of amino acid import via the ABC transporter GlnPQ determine the growth performance of Lactococcus lactis. J. Bacteriol. 198, 477-485 (2015).

38. Wolters, J. C. et al. Ligand binding and crystal structures of the substrate-binding domain of the ABC transporter OpuA. PLoS One 5, e10361 (2010).

39. Ferenci, T. The recognition of maltodextrins by Escherichia coli. Eur. J. Biochem. 108, 631-636 (1980).

40. McDevitt, C. A. et al. A molecular mechanism for bacterial susceptibility to zinc. PLoS Pathog. 7, e1002357 (2011).

41. Berntsson, R. P., Thunnissen, A. M., Poolman, B. & Slotboom, D. J. Importance of a hydrophobic pocket for peptide binding in lactococcal OppA. J. Bacteriol. 193, 4254-4256 (2011).

42. Ferenci, T., Muir, M., Lee, K. S. & Maris, D. Substrate specificity of the Escherichia coli maltodextrin transport system and its component proteins. Biochim. Biophys. Acta 860, 44-50 (1986).

43. Doeven, M. K., Abele, R., Tampe, R. & Poolman, B. The binding specificity of OppA determines the selectivity of the oligopeptide ATP-binding cassette transporter. J. Biol. Chem. 279, 32301-32307 (2004).

44. Oldham, M. L. & Chen, J. Crystal structure of the maltose transporter in a pretranslocation intermediate state. Science 332, 1202-1205 (2011).

45. Hor, L. I. & Shuman, H. A. Genetic analysis of periplasmic binding protein dependent transport in Escherichia coli. Each lobe of maltose-binding protein interacts with a different subunit of the MalFGK2 membrane transport complex. J. Mol. Biol. 233, 659-670 (1993).

46. Doeven, M. K., van den Bogaart, G., Krasnikov, V. & Poolman, B. Probing receptor-translocator interactions in the oligopeptide ABC transporter by fluorescence correlation spectroscopy. Biophys. J. 94, 3956-3965 (2008).

47. Hollenstein, K., Frei, D. C. & Locher, K. P. Structure of an ABC transporter in complex with its binding protein. Nature 446, 213-216 (2007).

48. Davidson, A. L., Shuman, H. A. & Nikaido, H. Mechanism of maltose transport in Escherichia coli: transmembrane signaling by periplasmic binding proteins. Proc. Natl. Acad. Sci. U. S. A. 89, 2360-2364 (1992).

49. Kapanidis, A. N. et al. Fluorescence-aided molecule sorting: analysis of structure and interactions by alternating-laser excitation of single molecules. Proc. Natl. Acad. Sci. U. S. A. 101, 8936-8941 (2004).

50. Lawrence, M. C. et al. The crystal structure of pneumococcal surface antigen PsaA reveals a metal-binding site and a novel structure for a putative ABC-type binding protein. Structure 6, 1553-1561 (1998).

51. Counago, R. M. et al. Imperfect coordination chemistry facilitates metal ion release in the Psa permease. Nat. Chem. Biol. 10, 35-41 (2014).

52. Begg, S. L. et al. Dysregulation of transition metal ion homeostasis is the molecular basis for cadmium toxicity in Streptococcus pneumoniae. Nat. Commun. 6, 6418 (2015).

53. Gould, A. D., Telmer, P. G. & Shilton, B. H. Stimulation of the maltose transporter ATPase by unliganded maltose binding protein. Biochemistry 48, 8051-8061 (2009).

54. Bao, H. & Duong, F. Discovery of an auto-regulation mechanism for the maltose ABC transporter MalFGK2. PLoS One 7, e34836 (2012).

55. Schuurman-Wolters, G. K., de Boer, M., Pietrzyk, M. K. & Poolman, B. Protein linkers provide limits on the domain interactions in the ABC importer GlnPQ and determine the rate of transport. J. Mol. Biol. 430, 1249-1262 (2018).

56. Speiser, D. M. & Ames, G. F. Salmonella typhimurium histidine periplasmic permease mutations that allow transport in the absence of histidine-binding proteins. J. Bacteriol. 173, 1444-1451 (1991).

57. Shevelev, I. V. & Hubscher, U. The 3' 5' exonucleases. Nat. Rev. Mol. Cell Biol. 3, 364-376 (2002).

58. Kotik-Kogan, O., Moor, N., Tworowski, D. & Safro, M. Structural basis for discrimination of L-phenylalanine from L-tyrosine by phenylalanyl-tRNA synthetase. Structure 13, 1799-1807 (2005).

59. Schmidt, A. et al. The quantitative and condition-dependent Escherichia coli proteome. Nat. Biotechnol. 34, 104-110 (2016).

60. Lycklama A Nijeholt, J. A., Vietrov, R., Schuurman-Wolters, G. K. & Poolman, B. Energy coupling efficiency in the Type I ABC transporter GlnPQ. J. Mol. Biol. 430, 853-866 (2018).

61. Borths, E. L., Poolman, B., Hvorup, R. N., Locher, K. P. & Rees, D. C. In vitro functional characterization of BtuCD-F, the Escherichia coli ABC transporter for vitamin B12 uptake. Biochemistry 44, 16301-16309 (2005).

62. Bok, J. W. & Keller, N. P. Fast and easy method for construction of plasmid vectors using modified quick-change mutagenesis. Methods Mol. Biol. 944, 163-174 (2012).

63. Vander Kooi, C. W. Megaprimer method for mutagenesis of DNA. Methods Enzymol. 529, 259-269 (2013).

64. Berntsson, R. P. et al. Selenomethionine incorporation in proteins expressed in Lactococcus lactis. Protein Sci. 18, 1121-1127 (2009).

65. Biemans-Oldehinkel, E. & Poolman, B. On the role of the two extracytoplasmic substrate-binding domains in the ABC transporter OpuA. EMBO J. 22, 5983-5993 (2003).

66. Schuurman-Wolters, G. K. & Poolman, B. Substrate specificity and ionic regulation of GlnPQ from Lactococcus lactis. An ATP-binding cassette transporter with four extracytoplasmic substrate-binding domains. J. Biol. Chem. 280, 23785-23790 (2005).

67. Geertsma, E. R., Nik Mahmood, N. A., Schuurman-Wolters, G. K. & Poolman, B. Membrane reconstitution of ABC transporters and assays of translocator function. Nat. Protoc. 3, 256-266 (2008).

68. Sung, C. K., Li, H., Claverys, J. P. & Morrison, D. A. An rpsL cassette, janus, for gene replacement through negative selection in Streptococcus pneumoniae. Appl. Environ. Microbiol. 67, 5190-5196 (2001).

69. Plumptre, C. D. et al. AdcA and AdcAII employ distinct zinc acquisition mechanisms and contribute additively to zinc homeostasis in Streptococcus pneumoniae. Mol. Microbiol. 91, 834-851 (2014).

70. Nir, E. et al. Shot-noise limited single-molecule FRET histograms: comparison between theory and experiments. J Phys Chem B 110, 22103-22124 (2006).

71. Lee, N. K. et al. Accurate FRET measurements within single diffusing biomolecules using alternating-laser excitation. Biophys. J. 88, 2939-2953 (2005).

72. Roy, R., Hohng, S. & Ha, T. A practical guide to single-molecule FRET. Nat. Methods 5, 507-516 (2008).

73. Rabiner, L. A. in Readings in speech recognition (ed Waibel, A. & Lee, K.) 267-29 (Morgan Kaufmann, 1990).

74. Baum, L. E. & Petrie, T. Statistical inference for probabilistic functions of finite state Markov chains. Annals of Mathematical Statistics 37, 1554-1563 (1966).

75. Viterbi, A. J. Error bounds for convolutional codes and an asymptotically optimum decoding algorithm. IEEE Trans. Inf. Theory 13, 260-269 (1967).